DISCLAIMER

Evaluation of 1/100-Scale Mooring Systems for Wave Energy Converters

Charles Candon, Thanh Toan Tran, Rebecca Fao,
Matthew Hall, and Stephen Chamot

National Laboratory of the Rockies

The National Laboratory of the Rockies is a national laboratory of the U.S. Department of Energy, Office of Critical Minerals and Energy Innovation, operated under Contract No. DE-AC36-08GO28308.

This report is available at no cost from the National Laboratory of the Rockies (NLR) at www.nlr.gov/publications.

Technical Report
NLR/TP-5700-98531
April 2026

NATIONAL
LABORATORY
OF THE ROCKIES

Evaluation of 1/100-Scale Mooring Systems for Wave Energy Converters

Charles Candon, Thanh Toan Tran, Rebecca Fao, Matthew Hall, and Stephen Chamot

National Laboratory of the Rockies

Suggested Citation
Candon, Charles, Thanh Toan Tran, Rebecca Fao, Matthew Hall, and Stephen Chamot. 2026. *Evaluation of 1/100-Scale Mooring Systems for Wave Energy Converters*. Golden, CO: National Laboratory of the Rockies. NLR/TP-5700-98531. https://www.nlr.gov/docs/fy26osti/98531.pdf.

The National Laboratory of the Rockies is a national laboratory of the U.S. Department of Energy, Office of Critical Minerals and Energy Innovation, operated under Contract No. DE-AC36-08GO28308.

This report is available at no cost from the National Laboratory of the Rockies (NLR) at www.nlr.gov/publications.

Technical Report
NLR/TP-5700-98531
April 2026

National Laboratory of the Rockies
15013 Denver West Parkway
Golden, CO 80401
303-275-3000 • www.nlr.gov

Acknowledgments

The authors would like to extend their sincere gratitude to National Laboratory of the Rockies technicians Mark Murphy and Kyle Swartz for their hard work, expertise, and dedication. Their hands-on skill and commitment to problem-solving have been instrumental in bringing this project from concept to reality.

List of Acronyms

CAD	computer-aided design
DAQ	data acquisition system
DOF	degrees of freedom
EDASS	EtherCAT Data Acquisition System Software
FDM	fused deposition modeling
FH	free-hanging
LC	load cell
NI	National Instruments
NLR	National Laboratory of the Rockies
OEM	original equipment manufacturer
PTO	power take-off
RM3	Reference Model 3
SEC	secured
SLA	stereolithography
SWEL	Sea Wave Environmental Lab
WEC	wave energy converter

Executive Summary

This study evaluates the feasibility, accuracy, and limitations of using 1/100-scale physical mooring systems to represent full-scale mooring behavior for wave energy converters (WECs) during small-scale tank testing. The work focuses on a point absorber WEC based on the Reference Model 3 device (Neary et al. 2014) deployed in conditions representative of the PacWave South test site and examines whether small-scale physical testing can reliably inform numerical modeling, design decisions, and future prototype development.

Four mooring configurations were designed at full scale: catenary chain, taut nylon, semitaut nylon, and semitaut polyester. These designs were then scaled using Froude scaling laws for implementation in the National Laboratory of the Rockies' Sea Wave Environment Lab wave tank. Due to geometric constraints, the mooring layouts were approximated with a two-line planar (fore–aft) system, providing equivalent longitudinal stiffness for unidirectional wave conditions.

Because accurate small-scale mooring representation is inherently challenging, significant effort was dedicated to materials selection and line fabrication. Despite careful construction, line mass densities, diameters, and stiffnesses could only be matched to within approximately 10%–20% of scaled design values, and larger deviations occurred for nylon ropes requiring multiple springs. Additional challenges arose from the observer effect, as load cells and instrument wiring introduced added mass, damping, and unintended forces that influenced WEC motion and anchor loads.

A comprehensive testing campaign included free-decay tests, forced-displacement tests, 81 wave-run tests across three wave conditions, and three unique load cell configurations (free-hanging, secured, and no load cell). Post-test load cell calibrations showed minimal calibration drift overall but revealed that one load cell experienced damage late in testing.

Numerical simulations using mid-fidelity numerical models were conducted to better understand the tank testing results. Specifically, the well-known open-source WEC modeling code WEC-Sim coupled to MoorDyn was used.

Across all mooring configurations, results demonstrated the following:

- Scaled mooring behavior is highly sensitive to small errors in stiffness, line length, and mass distribution, particularly at 1/100 scale.
- Load cell integration meaningfully altered mooring tensions and device dynamics, underscoring the difficulty of obtaining accurate small-scale load measurements without affecting the system.
- Device motions and mooring tensions varied widely between load cell configurations, highlighting the need for onboard or low-disturbance instrumentation approaches.
- Numerical modeling comparison indicates that there is some agreement depending on wave cases and mooring configurations.

Overall, this study concludes that small-scale (1/100) physical mooring models can provide valuable qualitative insights, including relative comparisons between mooring types and trends in device behavior, but cannot reliably replicate full-scale mooring loads or dynamic response

without significant scaling distortion. Physical tests at this scale are most appropriate for motion characterization and model validation within known limitations, not for deriving absolute mooring loads or final engineering design values.

Key lessons learned emphasize the importance of improved instrumentation strategies, iterative wave tank tuning, more precisely manufactured scaled mooring components, and enhanced anchoring systems to reduce experimental uncertainty. These findings will inform future small-scale testing campaigns, guide numerical model validation strategies, and support ongoing WEC development.

Table of Contents

List of Figures

List of Tables

1 Introduction

Wave tank testing is a critical step in the development of wave energy converter (WEC) designs because it provides a controlled environment to evaluate performance, survivability, and efficiency before deploying prototypes in the ocean. A wide range of sea states can be replicated in a tank that would be costly and difficult to consistently test at sea. Tank testing allows designers to validate numerical models, measure power capture, and assess hydrodynamic responses with high repeatability. It also helps identify design weaknesses early, reducing risk and saving resources by guiding design improvements prior to full-scale deployment. Ultimately, it bridges the gap between theory and real-world application, ensuring WEC technologies are both effective and reliable in harsh marine environments.

Challenges arise when attempting to accurately model and simulate full-scale mooring behavior at reduced scale. Mooring dynamics strongly influence device motions and loads, and inaccuracies in their representation can lead to suboptimal design decisions. It is therefore essential to recognize the limitations of scaled mooring experiments and to consider results accordingly. Understanding these limitations is critical for reliable model validation, device redesign, and eventual scale-up to field trials.

At small scales, such as those of the National Laboratory of the Rockies' (NLR's) Sea Wave Environmental Lab (SWEL) wave tank, accurately representing mooring systems is particularly challenging. Test results can be highly sensitive to seemingly minor inaccuracies in mooring line properties, including stiffness, density, and material choice. As smaller scales are reached, it is especially hard to integrate load cells in the system without affecting the dynamics of the mooring system. It is important to understand these challenges, establish best practices for minimizing their effects during experimental design, and develop appropriate approaches for interpreting results in light of these limitations.

Numerical modeling also plays an important role in WEC development, and it is therefore critical for numerical models to agree with results attained in tank testing. Numerical models may be validated through tank testing, but the physical model and test conditions must match the model input. This may be especially difficult at small scales and with a limited tank size.

The work covered in this report aims to test the feasibility of using physical models of small-scale (1/100) mooring systems to estimate mooring loads and simulate device behavior when testing WECs in a wave tank. The report aims to answer the question of whether it is practical to model mooring systems at this small of a scale. Experimental results will also be compared with numerical modeling results to compare two approaches for evaluating WEC mooring loads.

2 Background

To understand how well WEC mooring systems can be evaluated at small scales, we developed a realistic scenario using the SWEL wave tank at NLR, which is suitable for testing WEC prototypes between 1/75 and 1/100 scale. Since mooring design and setup can have a significant impact on the hydrodynamic performance of a device, a focused effort was undertaken to understand the limitations of this tank size for implementing realistic mooring setups and to develop best practices for moorings at small scale.

In this study, we compared results from experimental testing to numerical models of the same mooring scenario. We also ran mid-fidelity simulations using the open-source WEC-Sim software as well as high-fidelity computational fluid dynamics simulations using STAR-CCM+. By evaluating the agreement between these numerical methods and experimental methods, we drew conclusions regarding the effectiveness of testing mooring systems using a small-scale physical tank.

For this study, a point absorber WEC based on the Reference Model 3 (RM3) device from Neary et al. (2014) and deployed at the PacWave South site was considered. PacWave South is a pre-permitted grid-connected wave energy test facility off the coast of Oregon and offers relevant wave conditions to use as the basis for our tests. The sea state parameters considered for this study are based on the PacWave Resource Assessment (Dunkle et al. 2020) and are listed in Table 1.

Table 1. PacWave South Site Conditions

Parameter	Value
Water depth	70 m
Maximum current, 50-year return period	0.9 m/s
Largest wave, 50-year contour (period, height)	16 s, 13.2 m
Mean December wave (period, height)	11 s, 3.5 m
Mean August wave (period, height)	9 s, 1.75 m

The device under test for this experiment is based on the RM3 point absorber WEC. The RM3 was chosen because point-absorber-style WECs are one type of device that will likely be deployed at PacWave (Housner and Sirnivas 2023). Mooring systems designed for an RM3-style device at PacWave are likely to be similar to numerous real-world deployment scenarios.

The RM3 (diagrammed in Figure 1) was designed as part of a project led by Sandia National Laboratories in 2014 (Neary et al. 2014). The authors of the report describe the device as follows:

> *The RM3 wave point absorber, also referred to as a wave power buoy, was designed for a reference site located off the shore of Eureka in Humboldt County, California. The concept design for this device was inspired by the Ocean Power Technology's PowerBuoy (http://www.oceanpowertechnologies.com), which is a two-body floating point absorber (FPA) designed to convert ocean wave energy into electrical power.*

The design of the device consists of a surface float that translates (oscillates) with wave motion relative to a vertical column spar buoy, which connects to a subsurface reaction plate. This two-body point absorber converts wave energy into electrical power predominately from the device's heave oscillation induced by incident waves; the float is designed to oscillate up and down the vertical shaft up to 4 m. The bottom of the reaction plate is about 35 m below the water surface. The device is targeted for deployment in water depths of 40 m to 100 m. The point absorber is also connected to a mooring system to keep the floating device in position. Our RM3 design assumed a hydraulic PCC system, which is placed inside the vertical column. The optimum energy capture of a wave point absorber occurs when the system is at resonance, in other words, when the oscillating body velocity is in-phase with the hydrodynamic wave excitation force.

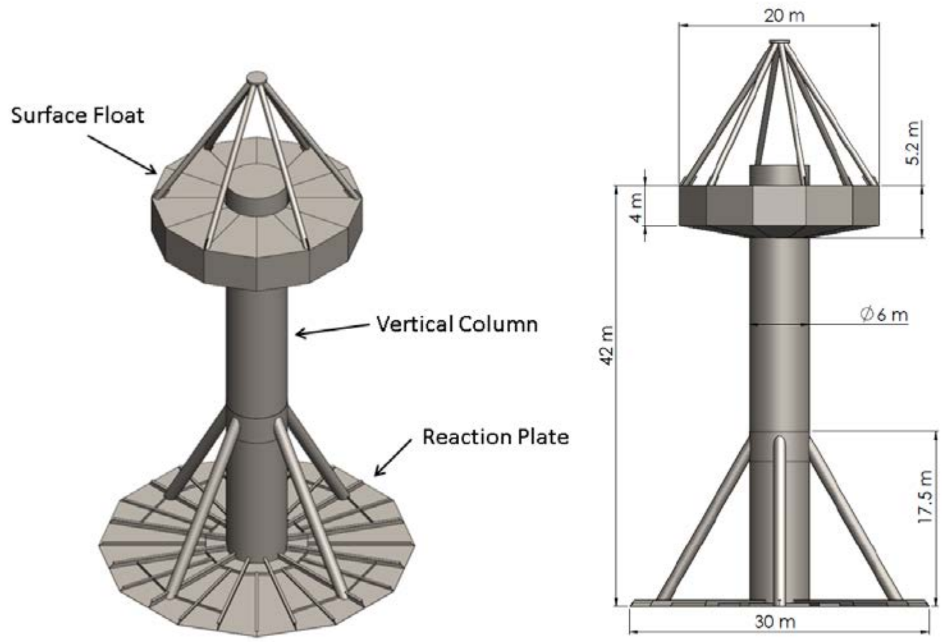

Figure 1. RM3 full-scale device design and dimensions.

Source: Neary et al. (2014)

3 Mooring System Design

The main goal of a mooring system is "station keeping," or keeping a floating structure in its desired position. This function is typically considered only in the horizontal plane, with the goal of keeping the horizontal displacement envelope of the floating structure (also called the watch circle) within certain bounds. Those bounds can be defined by requirements for navigation, a need for keeping multiple devices in relative position in an array, the motion tolerances of power cables, and more.

Mooring systems can also have additional goals, especially for wave and tidal energy converters. A few common examples are:

- Weathervaning: the mooring system should cause the floating system to passively orient itself to the incoming wave or current direction.
- Hydrostatic stability: the mooring system should provide stiffness in pitch and roll to the floating structure.
- Power take-off (PTO): the mooring system provides the reaction force against the structure's motion, which drives a power conversion mechanism.

The mooring system is also usually the sole means of providing yaw stability in a floating system. While this function is often a natural result of other functions and not design-driving, in some cases it can become a more significant factor.

A variety of mooring systems may be chosen depending on the type of WEC. Point absorbers may be moored by either a spread mooring system or a single-point mooring system. An RM3-like device would likely use a spread system to accommodate its heave motion. The spread mooring system can have any number of lines but most use three or four. The lines may have different configurations, including catenary, semitaut, or taut (Housner and Sirnivas 2023), and may be made of materials such as polyester, nylon, chain, or wire rope.

For this study, four mooring configurations were designed: catenary chain, taut nylon, semitaut polyester, and semitaut nylon. Each configuration was sized for the RM3 device at the PacWave South site, using quasi-static analysis and simplified assumptions about the current loads and wave-induced motions experience by the device. The model used in the design was MoorPy, a quasi-static mooring analysis library (Hall et al. 2021). Each mooring system was designed at full scale then scaled down to 1/100 scale using Freude scaling laws for implementation in the wave tank.

The mooring design approach assumes a steady horizontal drag force of $D = 223$ kN based on a conservative estimate of the drag force as given in Equation (1):

$$D = \frac{1}{2}\rho C_d A V^2 \tag{1}$$

where $\rho = 1{,}025$ kg/m^3 is the density of water, $C_d = 2$ is the drag coefficient, $A = 268$ m^2 is the cross-sectional area of the WEC, and $V = 0.9$ m/s is the maximum 50-year return period current velocity (Dunkle 2020). It should be noted that the density of seawater was used in the drag calculation while experimentation was conducted in fresh water.

Based on the largest wave on the 50-year contour with a wave period of $t = 16$ s and a wave height of h =13.2 m, the surge response amplitude operator, R, is estimated to be 0.6. The significant surge amplitude is estimated to be 4 m. The extreme surge amplitude (about the mean offset position) is assumed to be 10 m. This value is used when sizing the mooring systems for extreme loads.

Because of the dimensions of the wave tank (given in Section 4.3), three- and four-line mooring systems are not feasible to test. This study uses a two-dimensional approximation with a single fore and aft line. This configuration provides approximately the same restoring stiffness in the longitudinal direction as a three-line mooring system, because the stiffness of two lines spread laterally at 120 degrees is equivalent to the stiffness of one line down the center. Accordingly, this two-line planar approximation is sufficient for unidirectional waves, and the results can be used to approximate the response of a similar system with more lines.

3.1 Catenary Chain

The mooring lines of the catenary chain configuration each consist of a single chain connecting the WEC to an anchor. In its neutral position, most of the chain is resting on the seabed, and only during the most extreme sea state does the chain come almost completely off the seabed. To prevent the chain from contacting the heave plate, a float is added to the chain close to the WEC body. Figure 2 shows a single line in its neutral and extreme sea state conditions with Table 3 indicating the precise locations of points of interest on the plot. Table 2 gives the full-scale and tank-scale mooring line property outputs from MoorPy. As noted earlier, the mooring system implemented in the tank tests uses two of these mooring lines, one in front and one behind the WEC; however, the MoorPy model assumes three lines offset 120 degrees from each other.

Table 2. Catenary Chain Design Properties

Property	Full Scale	Tank Scale (1/100)
Neutral tension	55,554 N	0.056 N
Maximum tension	3,130,786 N	3.131 N
Line length	435.6 m	4.356 m
Line diameter	0.077 m	0.77 mm
Line mass	117.24 kg/m	11.72 g/m
Elastic stiffness	5.02E+08 N	501.75 N

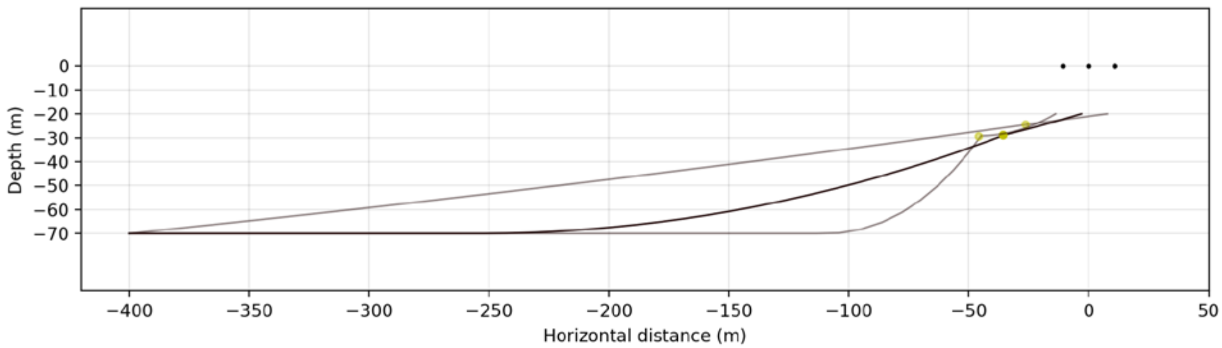

Figure 2. Catenary chain MoorPy design with WEC (black dots) in neutral position (middle dot), extreme negative surge position (left dot), and extreme positive surge position (right dot). The chains (black and gray lines) start at the fairlead connection points and end at the anchor point with inline floats (yellow dots).

Table 3. Catenary Chain Mooring Design Plot Points

Points	Positions (Horizontal Distance [m], Depth [m])
Anchor	(-397, -70)
WEC neutral position	(0, 0)
WEC positive position	(10.73, 0)
WEC negative position	(-10.77, 0)
Fairlead neutral position	(-3, -20)
Fairlead positive position	(7.73, -20)
Fairlead negative position	(-13.77, 20)

3.2 Taut Nylon

The taut nylon configuration consists of a single nylon line between the WEC and the anchor. The line is taut and does not contact the seabed while the device is at its neutral position. Figure 3 shows a single line in its neutral and extreme sea state conditions with Table 5 indicating the precise locations of points of interest on the plot. Table 4 gives the full-scale and tank-scale mooring line property outputs from MoorPy.

Table 4. Taut Nylon Design Properties

Property	Full Scale	Tank Scale (1/100)
Neutral tension	23,693 N	0.024 N
Maximum tension	490,269 N	0.490 N
Line length	398.2 m	3.982 m
Line diameter	0.066 m	0.66 mm
Line mass	2.57 kg/m	0.26 g/m
Elastic stiffness	4.88E+06 N	4.88 N

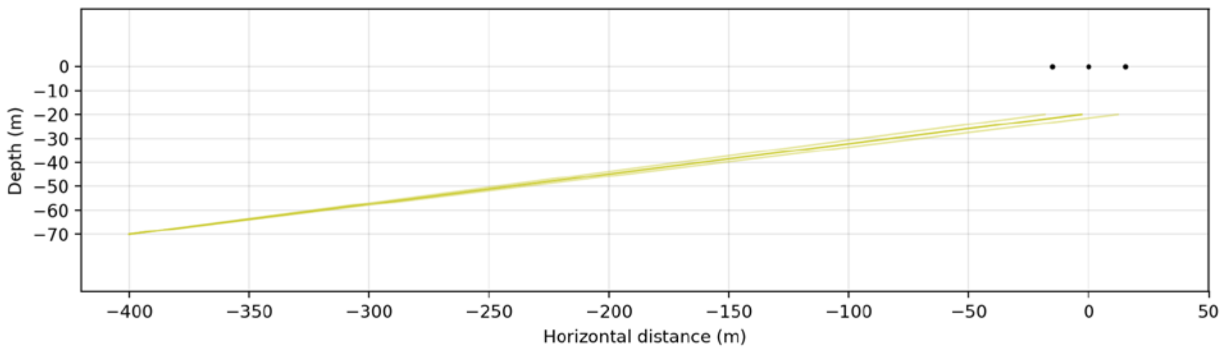

Figure 3. Taut nylon MoorPy design with WEC (black dots) in neutral position (middle dot), extreme negative surge position (left dot), and extreme positive surge position (right dot). The nylon lines (yellow) start at the fairlead connection points and end at the anchor point.

Table 5. Taut Nylon Mooring Design Plot Points

Points	Positions (Horizontal Distance [m], Depth [m])
Anchor	(-397, -70)
WEC neutral position	(0, 0)
WEC positive position	(15.27, 0)
WEC negative position	(-15.23, 0)
Fairlead neutral position	(-3, -20)
Fairlead positive position	(12.27, -20)
Fairlead negative position	(-18.23, -20)

3.3 Semitaut Nylon

The semitaut nylon configuration consists of a nylon line connecting the WEC to a float and a chain connecting the float to the anchor. The nylon line is taut when the WEC is at its neutral position, and the chain hangs from the float in a similar manner as in the catenary configuration. Figure 4 shows a single line in its neutral and extreme sea state conditions with Table 7 indicating the precise locations of points of interest on the plot. Table 6 gives the full-scale and tank-scale mooring line property outputs from MoorPy.

Table 6. Semitaut Nylon Design Properties

Property	Full Scale		Tank Scale (1/100)	
	Chain	Rope	Chain	Rope
Neutral tension	37,114 N	28,960 N	0.037 N	0.029 N
Maximum tension	630,008 N	627,020 N	0.630 N	0.627 N
Line length	145.0 m	256.4 m	1.450 m	2.564 m
Line diameter	0.072 m	0.075 m	0.72 mm	0.75 mm
Line mass	103.68 kg/m	3.25 kg/m	10.37 g/m	0.32 g/m
Elastic stiffness	4.44E+08 N	6.22E+06 N	443.74 N	6.22 N
Buoy net buoyancy	2,000 kg	-	2g	-

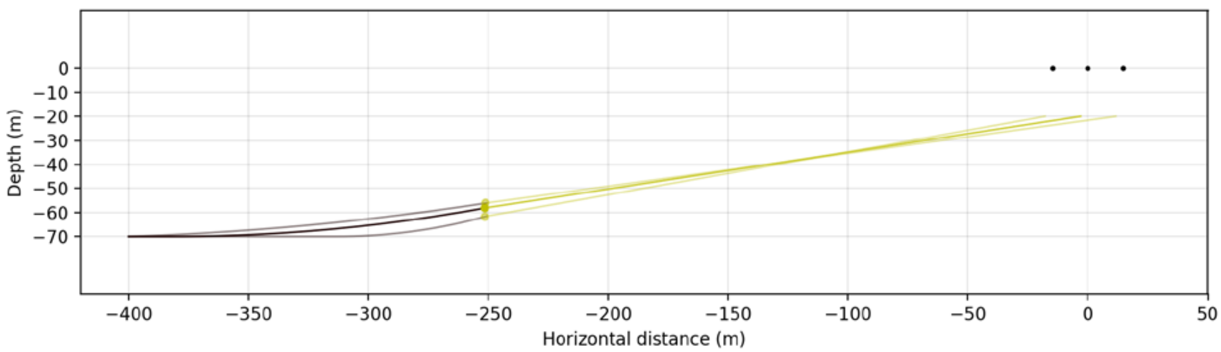

Figure 4. Semitaut nylon MoorPy design with WEC (black dots) in neutral position (middle dot), extreme negative surge position (left dot), and extreme positive surge position (right dot). The nylon lines (yellow) start at the fairlead connection points and end at the floats (yellow dots). The chains (black and gray lines) start at the float and end at the anchor point.

Table 7. Semitaut Nylon Mooring Design Plot Points

Points	Positions (Horizontal Distance [m], Depth [m])
Anchor	(-397, -70)
WEC neutral position	(0, 0)
WEC positive position	(14.79, 0)
WEC negative position	(-14.77, 0)
Fairlead neutral position	(-3, -20)
Fairlead positive position	(11.79, -20)
Fairlead negative position	(-17.77, -20)

3.4 Semitaut Polyester With Float

The semitaut polyester with float configuration consists of a polyester line connecting the WEC to a float and a chain connecting the float to the anchor. In the neutral position, the polyester line hangs from the WEC and is not taut. Figure 5 shows a single line in its neutral and extreme sea state conditions with Table 9 indicating the precise locations of points of interest on the plot. Table 8 shows the full-scale and tank-scale mooring line property outputs from MoorPy.

Table 8. Semitaut Polyester Design Properties

Property	Full Scale		Tank Scale (1/100)	
	Chain	Rope	Chain	Rope
Neutral tension	29,270 N	1,021 N	0.03 N	0.001 N
Maximum tension	2,304,699 N	2,298,655 N	2.30 N	2.299 N
Line length	389.6 m	46.6 m	3.90 m	0.466 m
Line diameter	0.091 m	0.120 m	0.91 mm	1.20 mm
Line mass	164.70 kg/m	9.78 kg/m	16.47 g/m	0.98 g/m
Elastic stiffness	7.05E+08 N	6.21E+07 N	704.88 N	62.09 N
Buoy net buoyancy	3,000 kg		3.00 g	

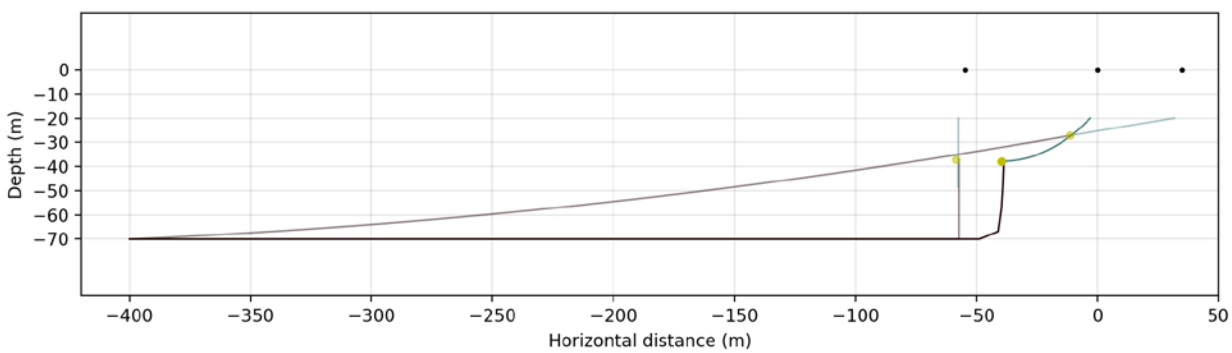

Figure 5. Semitaut polyester MoorPy design with WEC (black dots) in neutral position (middle dot), extreme negative surge position (left dot), and extreme positive surge position (right dot). The polyester lines (blue) start at the fairlead connection points and end at the floats (yellow dots). The chains (black and gray lines) start at the floats and end at the anchor point.

Table 9. Semitaut Polyester Mooring Design Plot Points

Points	Positions (Horizontal Distance [m], Depth [m])
Anchor	(-397, -70)
WEC neutral position	(0, 0)
WEC positive position	(34.74, 0)
WEC negative position	(-54.61, 0)
Fairlead neutral position	(-3, -20)
Fairlead positive position	(31.74, -20)
Fairlead negative position	(-57.61, -20)

4 Setup

4.1 RM3 Tank-Scale Model

The tank-scale WEC model is based on the RM3 device; however, there are differences in the design compared to the RM3 (Figure 6). The supporting struts that connect the reaction plate with the vertical column and the struts extending from the top of the float were omitted from the tank-scale model. Assuming a 1/100-scale factor, Table 10 shows the tank-scale model's deviation from the RM3 and Table 11 gives model properties. The larger dimensions of the tank-scale model were chosen to maximize energy capture in the NLR wave tank while still being able to manufacture the prototype with on-site rapid prototyping equipment. This study was not designed to validate the RM3 design; the RM3 design was simply used as baseline for the design of a tank-scale test article. The tank-scale model will continue to be referred to as the *RM3 model* due to its similarity to the reference design.

Table 10. Tank Model Deviation From Accurate RM3

Dimension	% Difference From True RM3
Float diameter	+37%
Heave plate diameter	+48%
Tube diameter	-4%
Heave plate to float distance	+7%

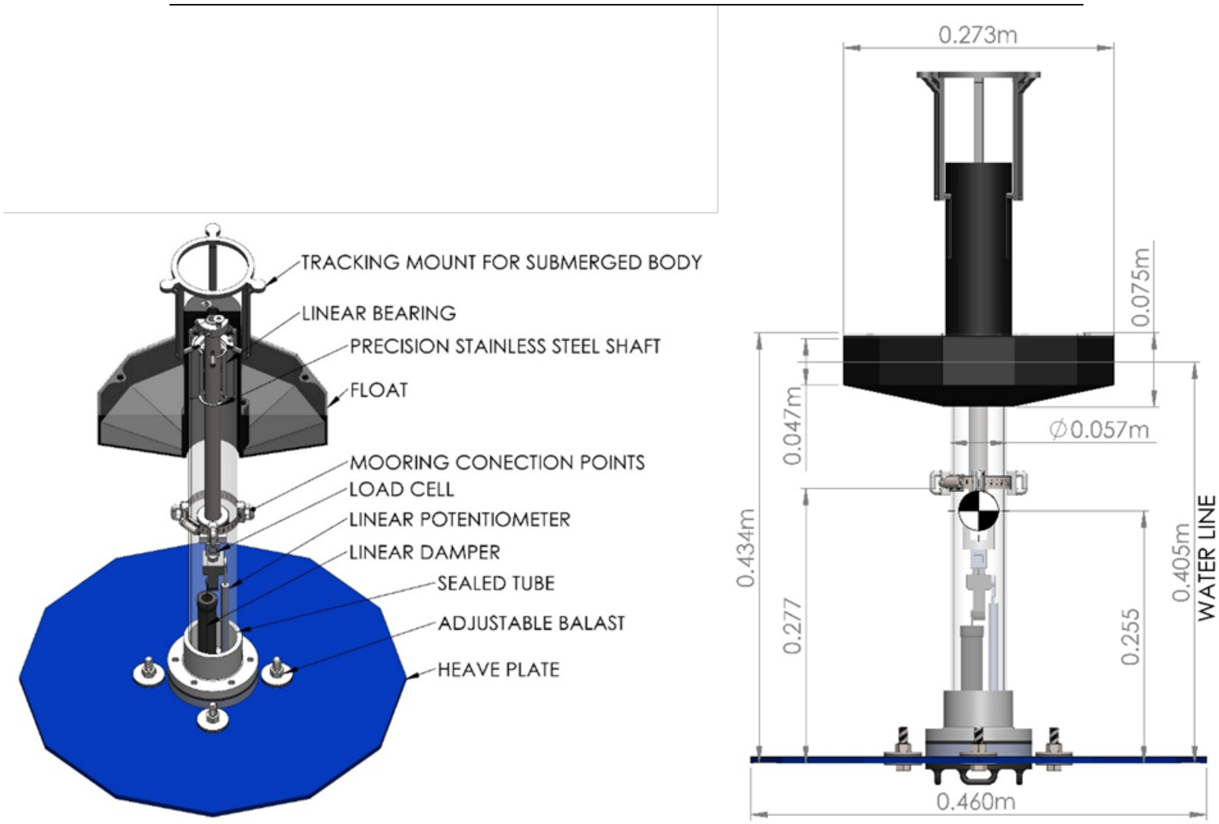

Figure 6. Tank-scale RM3 model as built

Table 11. RM3 Model Properties

Property	Value
Total mass	4.39 kg
Float assembly mass	1.57 kg
Heave assembly mass	2.82 kg
PTO travel	53.86
PTO damping	2,473 N·s/m

It is impossible to build the physical model to the exact specifications of the computer-aided design (CAD) model. Most notably, the mass of components will vary from their estimated mass in the CAD model. Linear dimensions will also vary but to a lesser extent. Additionally, the mooring line weight and load cell cable weights were not considered in the CAD model mass calculations. This variance will cause the computed draft length, center of gravity, center of buoyancy, and moments of inertia to vary slightly between the CAD model, which is used for numerical modeling, and the physical model used for tank testing. These differences will contribute to variance in the hydrodynamic performance between the numerical model and physical model.

The RM3 model was primarily fabricated using rapid prototyping equipment commonly available within the research community. Components requiring waterproofing, such as the float, were coated with West System epoxy. Smaller components were produced using a stereolithography (SLA) process, which inherently yields watertight parts. Applying an epoxy coating to 3D-printed parts is an effective method for minimizing water ingress (Murdy et al. 2024). The fabrication methods for each component and the materials used are outlined in Table 12.

Table 12. RM3 Model Manufacturing Methods

Component	Material	Fabrication Method
Float	Acrylonitrile styrene acrylate	3D printer (fused deposition modeling [FDM]) (sealed with West Systems epoxy)
Float top	Acrylic	Laser cutter
Face seal gaskets	Neoprene	Water jet
Heave plate	Acrylic	Laser cutter
Tracker mount	Cured resin	3D printer (SLA)
Precision linear shaft	Hardened steel	Lathe
Linear bearing adaptor	Cured resin	3D printer (SLA)
Sealed tube	Polycarbonate	Lathe
Load cell adaptor (upper)	Polyethylene terephthalate glycol (PETG)	3D printer (FDM)
Load cell adaptor (lower)	PETG	3D printer (FDM)
Bottom tube collar	Cured resin	3D printer (SLA)
Bottom sealing ring	Cured resin	3D printer (SLA)
Mooring attachment points	Onyx with chopped continuous carbon fiber reinforcement	3D printer (FDM with continuous fiber)

Lessons Learned

Model Building: 3D printing is a good option for building wave tank models. When printing FDM parts, coating parts in epoxy works well for waterproofing. For smaller parts that do not require much strength, SLA printing is convenient. When designing models, considering the instrumentation wire route early in the design process is important. If possible, it is best to design the instrument cables with connectors so that the cables can be removed from the model easily.

Mass Properties: Mass properties varied between the CAD model and the physical model. It is best to take precise measurements of the physical model as built and use those to update a version of the CAD model "as built". Additionally, the center of mass, center of buoyancy, and moments of inertia should be measured using a custom-built apparatus.

4.2 Instrumentation

Experimentation was conducted at NLR's SWEL. The lab is equipped with a wide range of instruments and features NLR-developed EtherCAT Data Acquisition Software (EDASS) running on a National Instruments (NI) PXIe-8135. NI 9239 modules are used for analog voltage measurements and NI 9237 modules are used for full-bridge strain gauge measurements. Strain sensors are excited by an external 10-volt rack-mounted power supply. See Appendix B for the specifications of each instrument.

The same model load cell was used for the PTO characterization, the mooring line tension measurements, and the mooring line spring constant characterization. The load cells were calibrated according to the OP1000 procedure with equipment traceable to SI units though the

National Institute of Standards and Technology by Futek, the original equipment manufacturer (OEM), in accordance with ANSI Z540-1, ISO 17025, ISO 9001, and ISO 13485.

Additionally, four above-water Qualisys Arqus A9 motion capture cameras were used to track the motion of each body in six degrees of freedom (6 DOF). These cameras were calibrated at the beginning of each day with the wand method as specified by the OEM.

4.3 Wave Tank

The tests were conducted in the NLR wave tank (Figure 7). A 1/100-scale factor was chosen based on the maximum wave amplitude that can be generated in the NLR wave tank (Table 13). At 1/100 scale, the PacWave 50-year contour extreme wave case (wave period 16 s and wave amplitude 13.2 m) can be reproduced. The tank does not have the ability to simulate current.

Table 13. Wave Tank Specifications

Property	Value
Wave maker	Flap type
Dimensions (L x D x W)	14 m x 1.3 m x 2.5 m
Capacity	13,000 gal
Wave amplitude	Up to 0.2 m
Wave period	0.5 to 5 s
Wave absorber	Quadratic curve beach

Figure 7. Model of NLR wave tank

To accurately simulate the 70-m PacWave water depth, the tank water depth was reduced to 0.7 m from its original 1.3 m. To achieve this, platforms were built to raise the effective tank floor (Figure 8). The platform's frames were constructed from extruded aluminum bar, and a high-density polyethylene sheet was fixed to the top of the platform to simulate the seabed. The platforms included six steel cables attached to lift points on the structure. The platforms were held in place with suction cups at each of the table legs. Two of these tables were installed in the tank, one fore and one aft of the device.

Suction cups attached to the platform's surface acted as the anchor points for each mooring line (Figure 9). Targets were marked on the surface of the platforms with permanent marker; then, after the tables were deployed in the tank, the mooring lines were attached to the suction cups, and the suction cups were placed on the target points using a gripping jaw retriever (McMaster PN 7294A38) prior to being installed in the tank. Additional fasteners were added in front of where the suction cups were placed to prevent the suction cups from sliding on the surface during extreme wave cases.

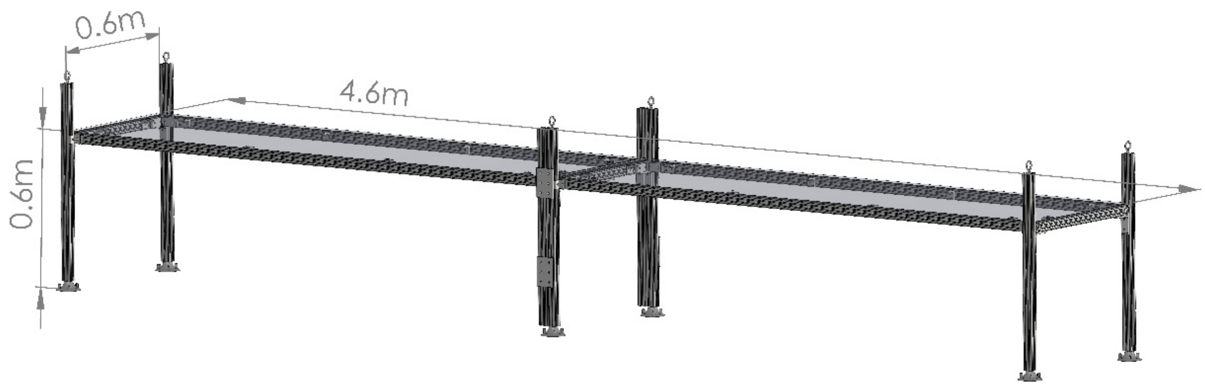

Figure 8. Wave tank seabed riser tables

Lessons Learned

Platform System: While the platform system was largely successful, a few things could be improved. Figure 10 shows the gap between the two platforms. An alternate design that eliminated this gap would be preferable since some catenary configurations require contact with the seabed along the entire span of the mooring line. As seen in Figure 10, the catenary line is slightly overhanging this gap. Fortunately for this test, the device drifted in the fore direction (to the right) before the system was loaded, so the gap did not affect the mooring line. The gap may also influence the performance of the heave plate because the volume of water beneath the heave plate varies when the device is over the gap versus over the table.

The vertical platform legs were made longer than necessary to allow the platform height to be adjusted for future tests. However, because these legs extend above the platform surface, they may contact the WEC. There would be more flexibility in the positioning of the WEC if these vertical legs did not extend above the platform surface.

Finally, the suction cup feet on the platforms were not ideal. They prevented the platforms from sliding on the tank floor; however, the suction cups flexed during large wave cases, causing the platforms to shift in the heave direction by 1–2 cm. While the effect of the shift was likely negligible on the experimental results, ideally, it would be eliminated. Using magnets or some other rigid attachment mechanism would be preferred.

Anchoring System: The suction cup anchoring system was not the ideal solution. They were difficult to place precisely on the platform from outside of the tank with the gripping jaw receiver. It was challenging to press down on the suction cup to get it to stick exactly in the intended location. Additionally, the load cell and instrument wire had to be managed. Since the load cells are exceptionally delicate, this procedure introduced a risk of damaging the load cells and causing them to vary from the OEM calibration. Rather than suction cups, a fixed mooring point would be better. However, this would require either entering the tank or removing the tables from the tank after each test. Additionally, the load cell instrument wire should be managed in a way that minimizes its influence on the load measurement. The wire running off the table may have added erroneous loads to the anchor tension measurements.

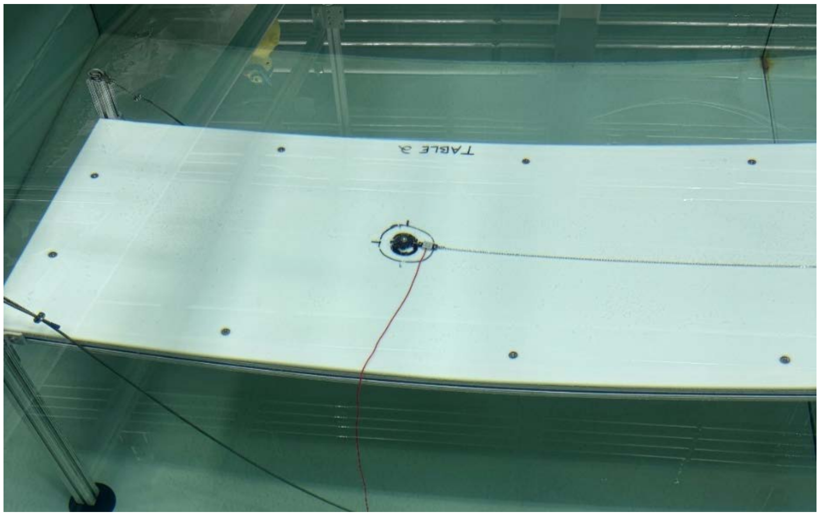

Figure 9. NLR wave tank with raised seabed platform and suction cup anchoring system. Note that the additional fasteners are not pictured here because they were added after the picture was taken.

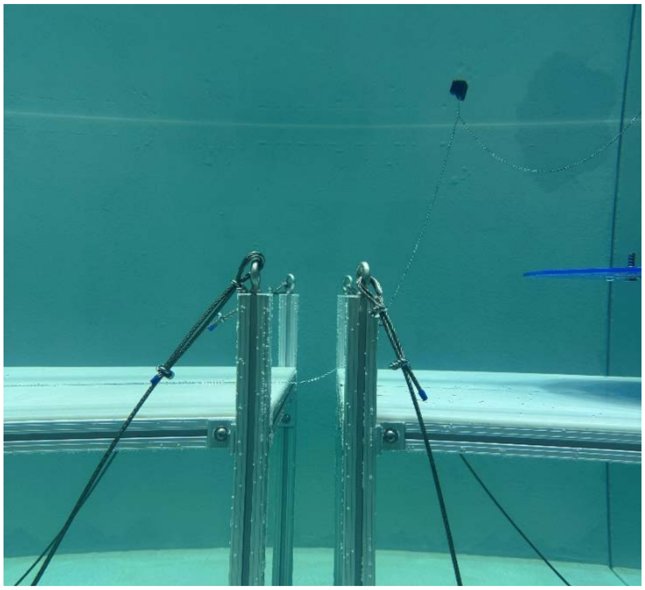

Figure 10. Gap between seabed platforms

4.4 Scaled Mooring System Construction

It is challenging to fabricate a scaled mooring line that precisely matches the geometric and material properties of the full-scale design using commonly available materials. Materials were selected to approximate the scaled properties as closely as possible. An example scale semitaut polyester with float mooring line model is shown in Figure 11.

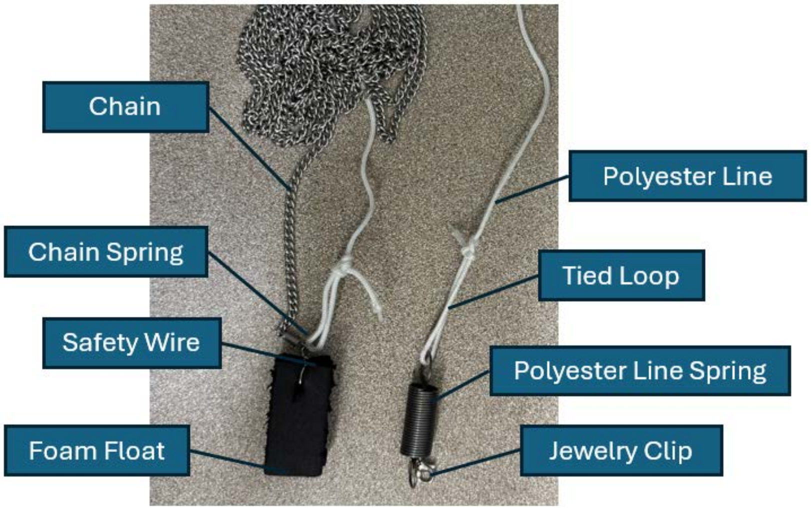

Figure 11. Scale semitaut polyester with float mooring line components

While searching for mooring line materials, we found that many vendors do not provide detailed mass, dimensions, or elasticity properties for the materials that may be used. So, a wide selection of materials was purchased, measured, and cataloged. The material with the closest properties to the design was chosen. Elasticity is one property that does not scale linearly with size, so springs with known spring constants were placed in series with the lines to approximate the Freude scaled elasticity. Custom springs with highly specific spring constants are available for order from online vendors. While the springs are necessary to adjust the elasticity of the lines, they add mass in areas that are not representative of the full-scale line. Additionally, the linear elasticity of the springs does not recreate the more complex nonlinear behavior of full-scale mooring lines.

The float was cut from a sheet of closed-cell foam with an estimated volume close to the design. The float was attached to the chain and polyester line with stainless steel safety wire. Once the mooring line was in place, the buoyancy of the float was adjusted by removing or adding material so that the line sat in the water appropriately.

At full scale, the polyester or nylon ropes would likely be terminated with a braided loop. However, for this study, a knot was used to join the rope with the float and spring (Figure 11). To achieve a precise length, the full lines were laid out on the ground next to a tape measure. An adjustable loop was then tied at the end of the lines to allow for fine adjustment of the line length. Polymer ropes change in length and elasticity when submerged, so these length measurements were conducted after submerging the ropes in water from the test tank for about 30 minutes.

The percentage variation of the properties of the fabricated mooring lines and the designed mooring lines are shown in Table 14. For this comparison a single line from each case was considered. Most of the mass, dimensional, and elasticity properties are within 15% of the accurately scaled values. Accurately scaled polyester and nylon ropes with accurate diameters and linear densities were difficult to find. The especially large discrepancy between the taut nylon full line masses is due to the addition of springs in series with the nylon line. To produce a line with the appropriate spring constant, four springs were added in parallel with the already lightweight nylon line. These springs were added at the connection point to the WEC (Figure 12).

While it is important to scale all properties of the mooring lines accurately, it is usually impractical to reproduce a full-scale mooring system exactly. It was determined that for the chain, the linear mass density was the most important property to accurately scale, and for the nylon and polyester ropes, the elasticity (spring constant) was the most important property to scale accurately. These properties are the main determining factors that contribute to the restoring force on the WEC. Each of the constructed mooring line configurations is shown in Figure 12.

Table 14. Mooring Line Properties

(% deviation from design)

Property	Semitaut Nylon	Semitaut Polyester	Catenary Chain	Taut Nylon
Nominal chain diameter	-6.94%	-14.05%	-12.91%	-
Chain linear mass density	-10.86%	-14.33%	10.93%	-
Rope diameter	-10.08%	27.50%	-	17.67%
Rope linear mass density	10.89%	58.89%	-	42.42%
Full line mass (with springs)	-5.21%	-10.61%	13.56%	190.05%
Full line spring constant	-3.99%	9.31%	-21.33%	-1.65%

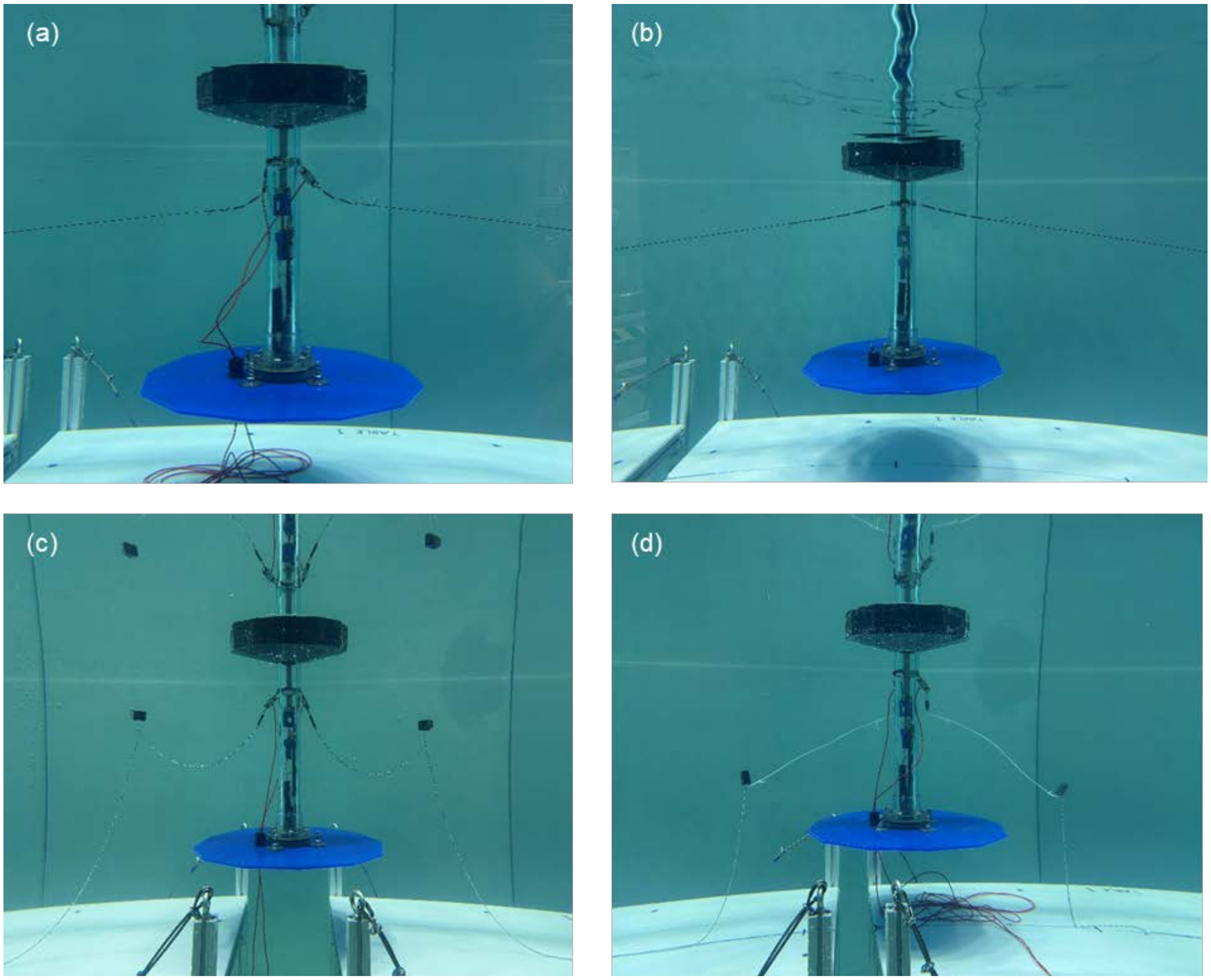

Figure 12. Deployed mooring configurations: (a) semitaut nylon, (b) taut nylon, (c) catenary with float, (d) semitaut polyester

Lessons Learned

Mooring Line Construction: Accurately scaled mooring line materials are difficult to find. To produce a more accurately scaled model, custom line and chain should be sourced or fabricated. Connection points between the mooring lines and other components are difficult to recreate accurately at small scales. The terminations of the rope lines should be glued loops rather than tied knots. An iterative design approach should be taken to more accurately match the target elasticity of the lines. Some materials change length and properties when submerged, which must be considered when constructing the lines.

4.5 Load Cell Configurations

Load cells (LC) were placed in series with the mooring lines to determine the loads on the anchors (LC1, LC3) and on the WEC (LC2, LC4). The locations of these load cells and the convention used for the fore and aft directions, which is referenced throughout this paper, are shown in Figure 13.

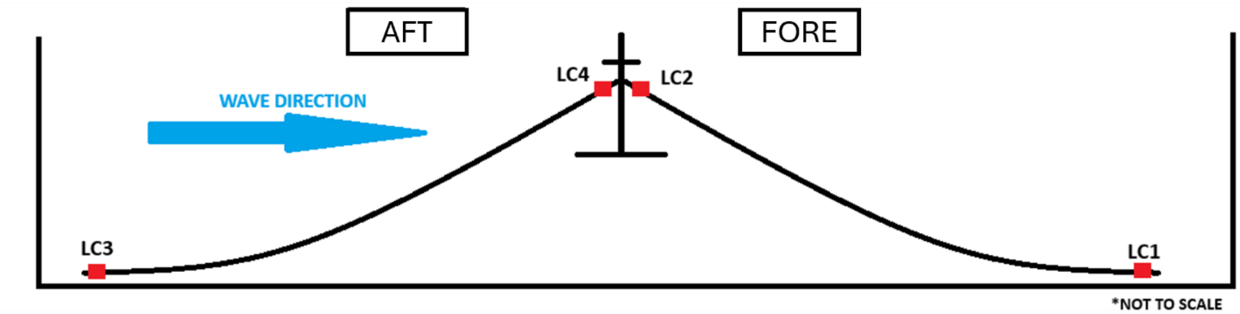

Figure 13. Load cell numbering scheme and fore/aft convention

The results of these tests are susceptible to the observer effect, in which the addition of measurement instrumentation influences the very quantities being measured. In this case, the integration of load cells inherently alters the system dynamics and response. Similar to the springs, the load cells introduce additional weight to the mooring line and create a short section with different stiffness characteristics compared to the intended line material.

The load cell wiring also contributes to these effects. The wires add mass and hydrodynamic and mechanical damping to the WEC, and because they extend to the DAQ system outside the tank, they can exert unintended, variable forces on the WEC. As shown in Figure 9, the load cell wire additionally influences the anchor load measurement by applying a constant lateral force resulting from the wire drooping off the platform edge.

To minimize these effects, additional slack in the instrument wires was placed on the platform directly below the WEC. This arrangement was intended to direct most of the wire-induced force in the heave direction while minimizing sway and surge forces. However, precisely and repeatably achieving this configuration was challenging, and some residual lateral forces remained.

To better understand the influence of load cells and identify an optimal configuration, three setups were tested:

1. **Free-hanging configuration:** Load cell cables hang freely from the load cells to the heave plate, where they are secured via a cable gland pass-through.
2. **Secured configuration:** Cables are fixed to the WEC near the load cells using zip ties.
3. **No-load-cell configuration:** Load cells are removed from the WEC side but retained on the anchor side. Additional mooring line length was added to compensate for the removed load cells.

Each load cell configuration is shown in Figure 14. Note that the secured load cell configuration was only tested with the catenary-with-float-line configuration. The free-hanging and no-load-cell configurations were tested with all four line configurations.

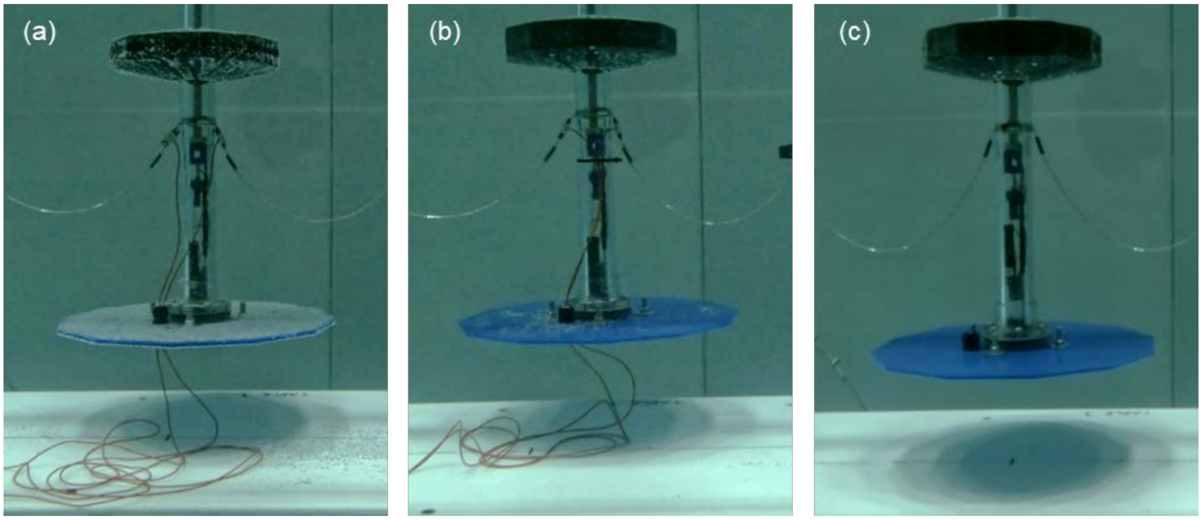

Figure 14. (a) Free-hanging, (b) secured, and (c) no-load-cell configurations

Lessons Learned

Instrumentation Cable Routing: Integrating load cells in line with the mooring lines proved to be especially difficult. For the anchor-side load cells, the wires could be fixed to the platform to reduce the effect of the weight of the cable on the load measurement. For the WEC-side load cells, it would be nearly impossible to run wires from the WEC to an external DAQ without influencing the test articles motion in some way. Integrating an onboard DAQ into the device could be one solution. In addition to these measures, the load cells should be tared while in place without any mooring line installed to compensate for the load cell wire weight and any other effects.

5 Procedures

5.1 Mooring Line Spring Constant Measurement

The spring constant for each of the mooring lines, with the additional springs in series, were measured. The full lines were laid on the concrete floor of the lab next to an extended tape measure. One end of the line was secured to a fixed point. The free end was then displaced by hand to four distances measured on the adjacent tape measure. The line was held at each of these displaced locations so that a steady-state load could be measured by the load cells. The polymer lines (nylon and polyester) were tested both dry and after being submerged in water from the test tank for about 30 minutes. Each line was displaced according to Table 15.

Table 15. Spring Constant Testing Schedule

Line Type	Line Configuration			Displacement Values (cm)			
Catenary	w/ LC	Fore lead	Dry	2	4	6	-
Catenary	w/ LC	Aft lead	Dry	2	4	6	-
Semitaut nylon w/ float	w/ LC	Fore lead	Dry	2	4	8	10
Semitaut nylon w/ float	w/ LC	Fore lead	Wet	4	8	10	14
Semitaut nylon w/ float	w/o LC	Fore lead	Dry	2	4	8	10
Semitaut nylon w/ float	w/o LC	Fore lead	Wet	4	8	10	14
Semitaut nylon w/ float	w/ LC	Aft lead	Dry	2	4	8	10
Semitaut nylon w/ float	w/ LC	Aft lead	Wet	4	8	10	14
Semitaut nylon w/ float	w/o LC	Aft lead	Dry	2	4	8	10
Semitaut nylon w/ float	w/o LC	Aft lead	Wet	4	8	10	14
Semitaut polyester w/ float	w/ LC	Fore lead	Dry	1	1.5	2	3
Semitaut polyester w/ float	w/ LC	Fore lead	Wet	1	2	3	4
Semitaut polyester w/ float	w/ LC	Aft lead	Dry	1	1.5	2	3
Semitaut polyester w/ float	w/ LC	Aft lead	Wet	1	2	3	4
Semitaut polyester w/ float	w/o LC	Fore lead	Dry	1	1.5	2	3
Semitaut polyester w/ float	w/o LC	Fore lead	Wet	1	2	3	4
Semitaut polyester w/ float	w/o LC	Aft lead	Dry	1	1.5	2	3
Semitaut polyester w/ float	w/o LC	Aft lead	Wet	1	2	3	4
Taut nylon	w/ LC	Fore lead	Dry	25	50	75	100
Taut nylon	w/ LC	Fore lead	Wet	20	40	60	80
Taut nylon	w/ LC	Aft lead	Dry	25	50	75	100
Taut nylon	w/ LC	Aft lead	Wet	20	40	60	80
Taut nylon	w/o LC	Fore lead	Dry	25	50	75	100
Taut nylon	w/o LC	Fore lead	Wet	20	40	60	80
Taut nylon	w/o LC	Aft lead	Dry	25	50	75	100

Line Type	Line Configuration			Displacement Values (cm)			
Taut nylon	w/o LC	Aft lead	Wet	20	40	60	80

5.2 PTO Damping Coefficient Determination

To determine the damping coefficient of the PTO, the device was subjected to three wave cases, and data from the onboard linear potentiometer and load cell were collected. Each wave case was repeated three times. For these tests, an umbilical cable was run from the top of the device to the DAQ. This cable significantly influences device motion, so it was removed for all other tests that did not require PTO measurements. Table 16 displays a damping coefficient test matrix.

Table 16. Damping Coefficient Test Matrix

Test Number	Wave Height (mm)	Wave Period (s)
1	75	1
2	75	1
3	75	1
4	100	2
5	100	2
6	100	2
7	125	1.75
8	125	1.75
9*	125	1.75

*Data from test number 9 were omitted due to measurement errors.

5.3 Wave Tank Characterization

The wave tank was run without the WEC installed to characterize the wave profile that is incident on the device once installed. This characterization was performed both with and without the mooring platforms installed to characterize the effect the tables have on the wave profile. The three regular wave cases that were run, herein referred to as the *wave cases,* are shown in Table 17.

Table 17. Wave Cases

Name	Wave Height	Wave Period
August mean wave at PacWave South (1/100 scale)	17.5 mm	0.9 s
December mean wave at PacWave South (1/100 scale)	35 mm	1.1 s
Maximum 50-year wave at PacWave South (1/100 scale)	132 mm	1.6 s

Each of these cases was run for 1 minute, and the wave heights were measured with the four ultrasonic wave height sensors. After each wave run, the tank was left to settle until the average wave height measured by the wave gauges was less than 1 mm. This took between 5 and 10 minutes, depending on the wave case run.

5.4 Device Installation

First, the mooring platforms were installed in the tank. Using an overhead crane, the platforms were lowered into the tank. To ensure the tables were placed in the correct position, measurements were taken on the tank wall, and the tables were aligned with these marks. The intended locations of the anchor points for each mooring system were marked on the tables.

Next, the WEC-side mooring lines were connected to the WEC, and the device was placed in the tank. The other ends of the lines were attached to the anchor suction cups. Using a gripping jaw retriever (McMaster PN 7294A38), the anchor-point suction cups were placed on the marked locations on the platforms.

Finally, the device was moved into its approximate position in the center of the tank with the gripping jaw retriever. Additional slack of the mooring line cables was gathered and placed under the device on the platform. The device was then left to settle into its neutral position by the natural restoring force of the mooring system.

5.5 Free Decay

For each mooring configuration, free-decay tests were conducted in all 6 DOF. After starting the data acquisition, the device was displaced in each DOF using the gripping jaw retriever. The device was then left to return to its neutral position by the restoring force of the mooring system. This procedure was repeated three times for each DOF.

5.6 Forced Displacement

Forced-displacement tests were conducted for each mooring configuration in the fore and aft directions. Using the gripping jaw retriever, the device was held at a position either fore or aft of its neutral position, and the tension on each mooring line was recorded. This was repeated three times in each direction.

5.7 Wave Runs

Three repetitions were run for each combination of mooring line configuration, load cell configuration, and wave case shown in Table 18, totaling 81 tests. In addition to data collected from the wave height sensors, mooring line load cells, and Qualisys motion capture system, video was taken with a GoPro action camera through the glass wall of the tank. After each wave run, the tank was left to settle until the average wave height was below 1 mm. The device was also manually returned to its neutral position, then left to settle before the next test.

Table 18. Wave Case Test Matrix

Test #	Line Configuration	Load Cell Configuration	Wave Height	Wave Period
1	Catenary with float	Free-hanging	132 mm	1.6 s
2	Catenary with float	Free-hanging	35 mm	1.1 s
3	Catenary with float	Free-hanging	17.5 mm	0.9 s
4	Catenary with float	No load cell	132 mm	1.6 s
5	Catenary with float	No load cell	35 mm	1.1 s
6	Catenary with float	No load cell	17.5 mm	0.9 s
7	Catenary with float	Secured	132 mm	1.6 s
8	Catenary with float	Secured	35 mm	1.1 s
9	Catenary with float	Secured	17.5 mm	0.9 s
10	Taut nylon	Free-hanging	132 mm	1.6 s
11	Taut nylon	Free-hanging	35 mm	1.1 s
12	Taut nylon	Free-hanging	17.5 mm	0.9 s
13	Taut nylon	No load cell	132 mm	1.6 s
14	Taut nylon	No load cell	35 mm	1.1 s
15	Taut nylon	No load cell	17.5 mm	0.9 s
16	Semitaut polyester	Free-hanging	132 mm	1.6 s
17	Semitaut polyester	Free-hanging	35 mm	1.1 s
18	Semitaut polyester	Free-hanging	17.5 mm	0.9 s
19	Semitaut polyester	No load cell	132 mm	1.6 s
20	Semitaut polyester	No load cell	35 mm	1.1 s
21	Semitaut polyester	No load cell	17.5 mm	0.9 s
22	Semitaut nylon	Free-hanging	132 mm	1.6 s
23	Semitaut nylon	Free-hanging	35 mm	1.1 s
24	Semitaut nylon	Free-hanging	17.5 mm	0.9 s
25	Semitaut nylon	No load cell	132 mm	1.6 s
26	Semitaut nylon	No load cell	35 mm	1.1 s
27	Semitaut nylon	No load cell	17.5 mm	0.9 s

5.8 Load Cell Post-Calibration

After the testing campaign concluded, the load cells were recalibrated in the lab. Twelve weights between 8.1 and 453 g were weighed on a high-precision scale to the nearest 1E-4 g. Each load cell was then hung from a piece of steel Unistrut fixed to the side of the tank. The load cell was attached to the steel Unistrut by a piece of safety wire wrapped into a loop and fixed to the load cell with an M3 fastener. The same safety wire method was used to hang the weights from the load cell. The cell cable was also fixed to this structure to provide strain relief and to attempt to minimize its influence on the force measurements. The weights were hung by the load cell according to Table 19.

Table 19. Load Cell Calibration Schedule

Number	Weight (g)
1	0
2	8.1472
3	18.089
4	20.0327
5	25.2272
6	35.1501
7	54.9203
8	104.9137
9	306.7381
10	444.9472
11	646.7716
12	898.4472
13	8.1472
14	0

At each load number, the weight was left to hang for approximately 5 s to allow for a stable voltage to be recorded.

6 Data Processing

6.1 Wave Height Data

Wave height and mooring load data were collected with EDASS at 1,000 Hz and saved in TDMS files. Raw data from the ultrasonic wave gauges are shown in Figure 15.

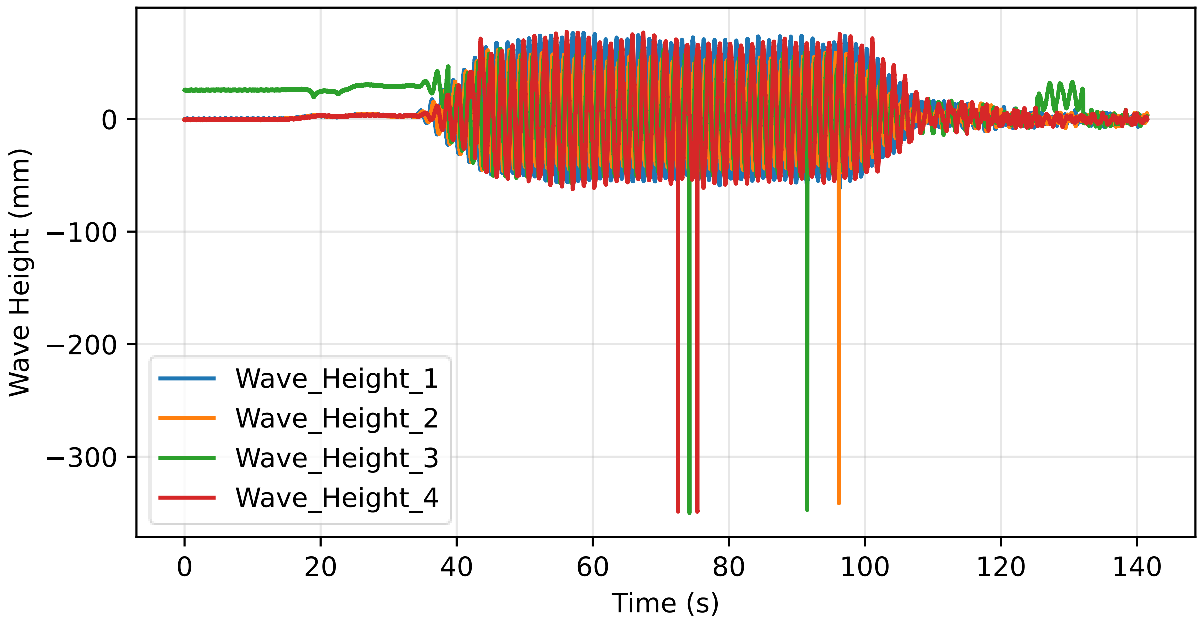

Figure 15. Unfiltered wave height data with spikes

The ultrasonic wave gauges sometimes miss samples, which manifests in the data as large spikes. Five of these spikes are shown in Figure 15. To remove these spikes, all points in the series greater than 100 or less than -100 were removed, and the remaining space was filled with a linear interpolation. Wave Gauge 3 was not considered because the WEC was directly below this gauge and sometimes caused interference with the sensor.

The ultrasonic wave gauges update at 20 Hz while the DAQ samples this signal at 1,000 Hz. The captured data file therefore has a stair-step pattern (Figure 16). By applying a fourth-order Butterworth low-pass filter with a 5-Hz cutoff, this signal is smoothed (Figure 17).

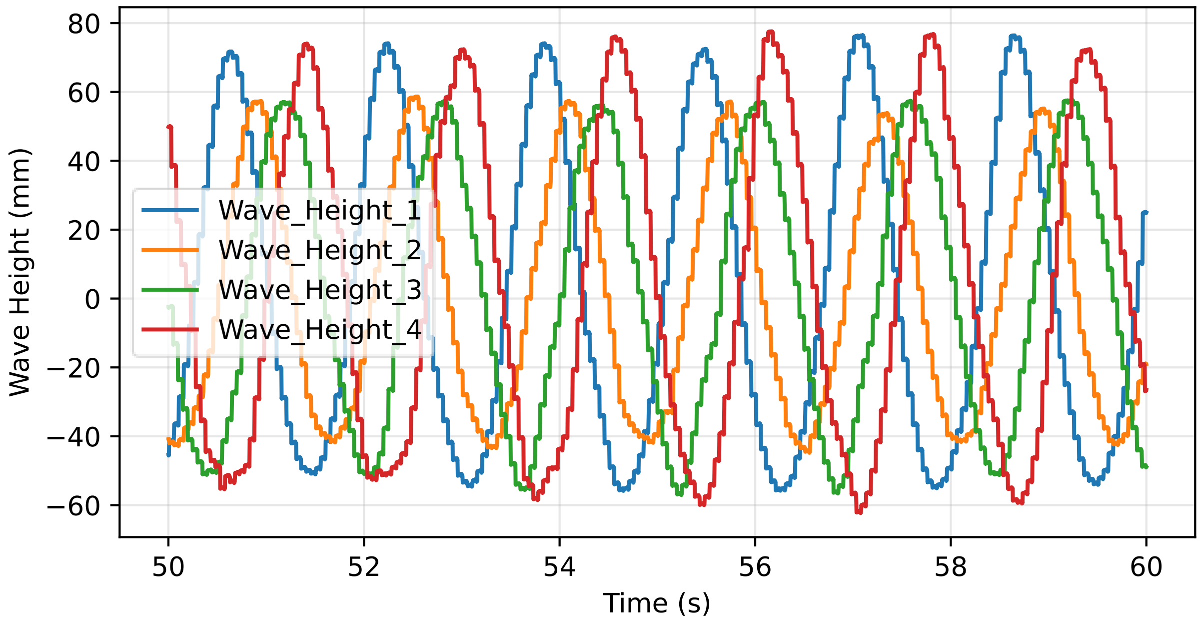

Figure 16. Unfiltered wave height data stair-step pattern

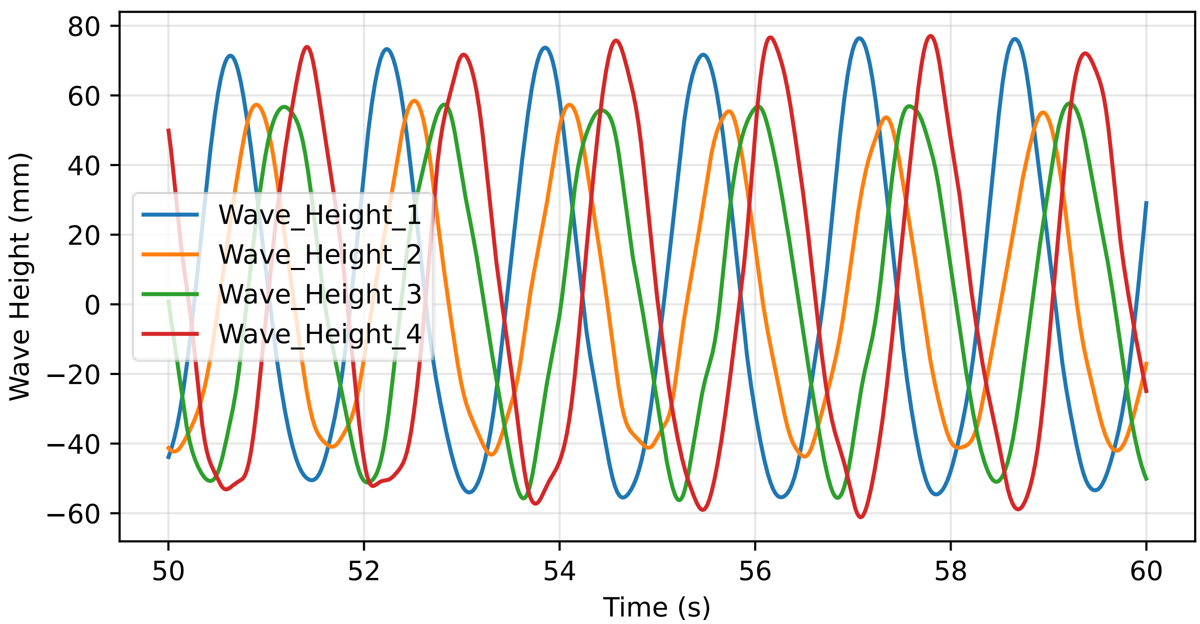

Figure 17. Filtered wave height data

A window of data where the wave height was relatively stable was then selected between the ramp-up and ramp-down period of the wave profile. Using a peak-finding algorithm on the filtered data, each peak and valley was identified. Wave heights were calculated by taking the difference between successive peaks and valleys. Similarly, wave periods were determined by calculating the time between successive peaks. The average of these values over a selected window after the wave ramp-up period was then calculated and reported.

6.2 Mooring Load Data

Raw load data from the four mooring line load cells sampled at 1,000 Hz are shown in Figure 18.

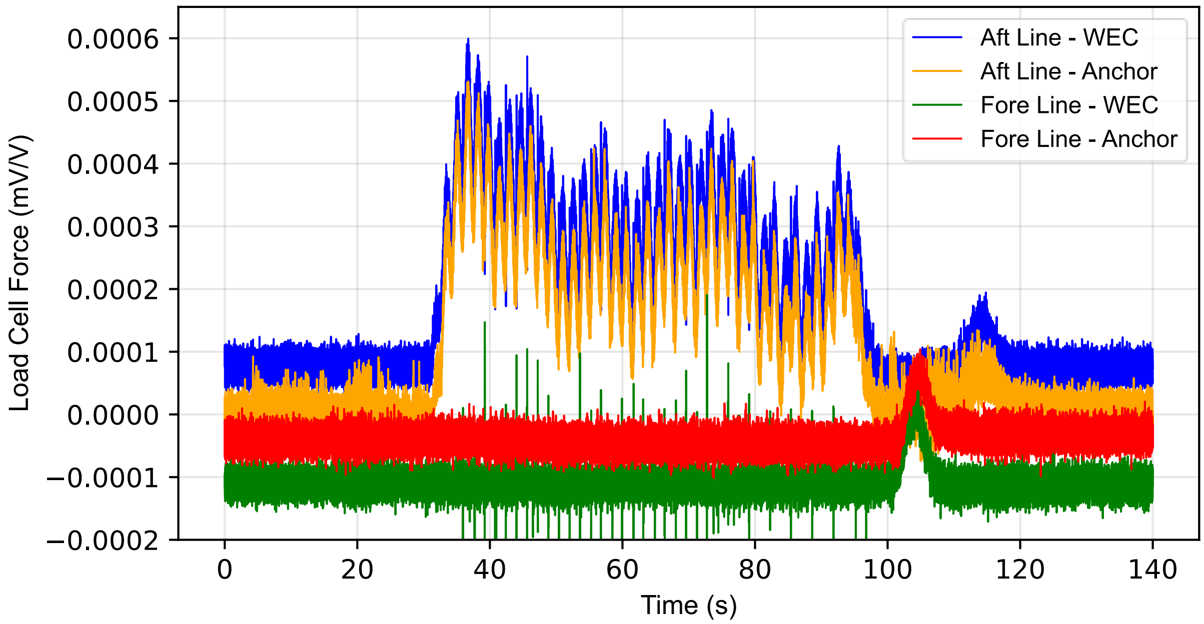

Figure 18. Raw mooring load data example

The raw load cell data contain high-frequency noise, which was filtered with a fourth-order Butterworth filter with a cutoff frequency of 5 Hz (Figure 19). The data were also scaled to newtons according to the OEM calibration certificate.

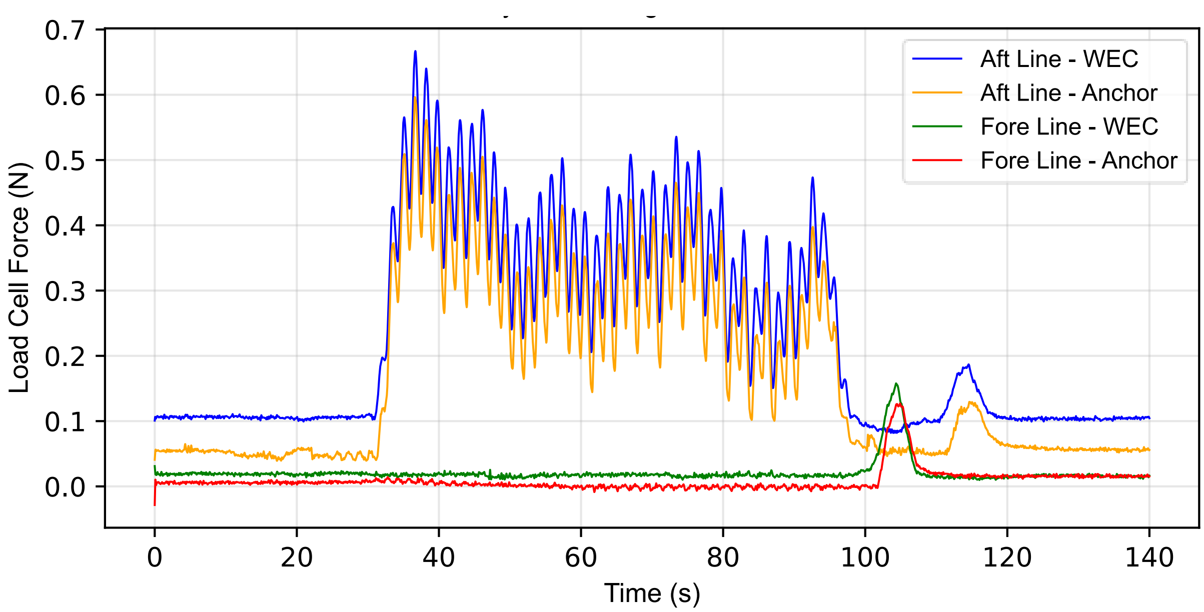

Figure 19. Filtered and scaled mooring load data example

From the filtered data, the average tension was calculated over a steady period before any waves were introduced. This value represents the neutral tension at each line connection point. A peak-finding algorithm was then applied to identify the local maxima of the sinusoidal loading signal over each period. The SciPy signal processing peak-finding function was used with the following parameters: distance = 100, width = 50, and prominence = 0.01% of the mean signal amplitude. From these detected peaks, the mean, median, and maximum tension values were determined for the range between the wave ramp-up and ramp-down periods. Additionally, the difference between the neutral tension and the absolute maximum was calculated. This compensates for irregularities in the neutral tensions between tests (See Section 7.4 for explanation).

The time when the first wave hits the device is an important region of interest. In the case of the extreme waves, the first few waves move the device from its neutral position to the extreme point of the mooring system. Consequently, the highest mooring load is usually soon after initial wave contact. The time between first contact and the peak mooring load was calculated for each extreme case and for the anchor load cell only. This was done manually by estimating the point when the first wave contacted the device. An example of this time period for each configuration is shown in Figure 20.

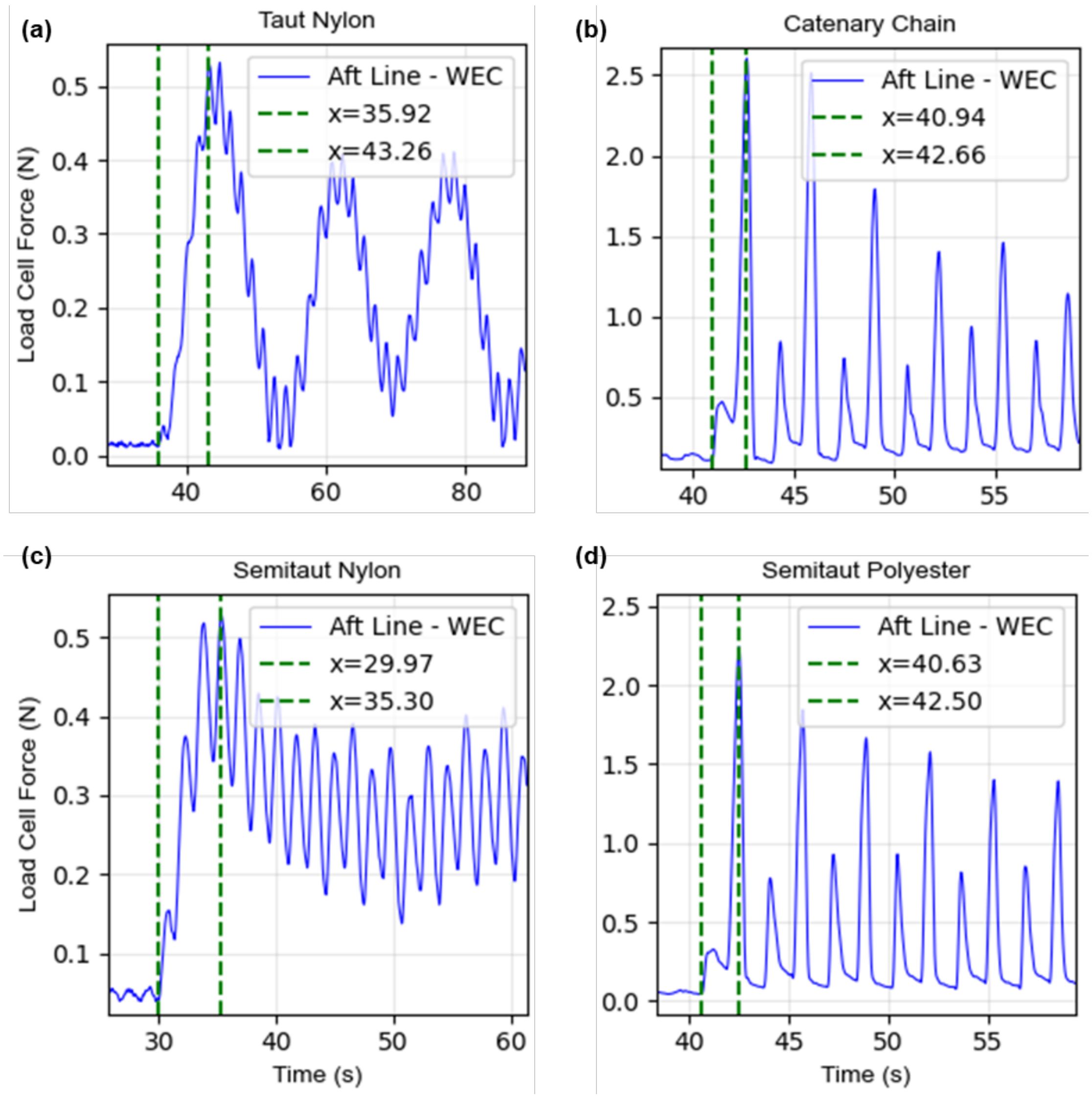

Figure 20. Example bounds for rise time from neutral tension to initial maximum calculation for (a) taut nylon, (b) catenary chain, (c) semitaut nylon, and (d) semitaut polyester

6.3 Qualisys Motion Data

The Qualisys motion capture system records the 6-DOF position and orientation for both the heave plate and float bodies at 240 Hz. The raw data contain gaps where the system loses tracking on a body. These gaps can be identified by consecutive samples that change rapidly. Once identified, the gaps are removed and replaced with linear interpolation. The gap-filled data are then filtered with a fourth-order Butterworth filter with a cutoff frequency of 3 Hz to smooth small amounts of jitter in the signal (Figure 21).

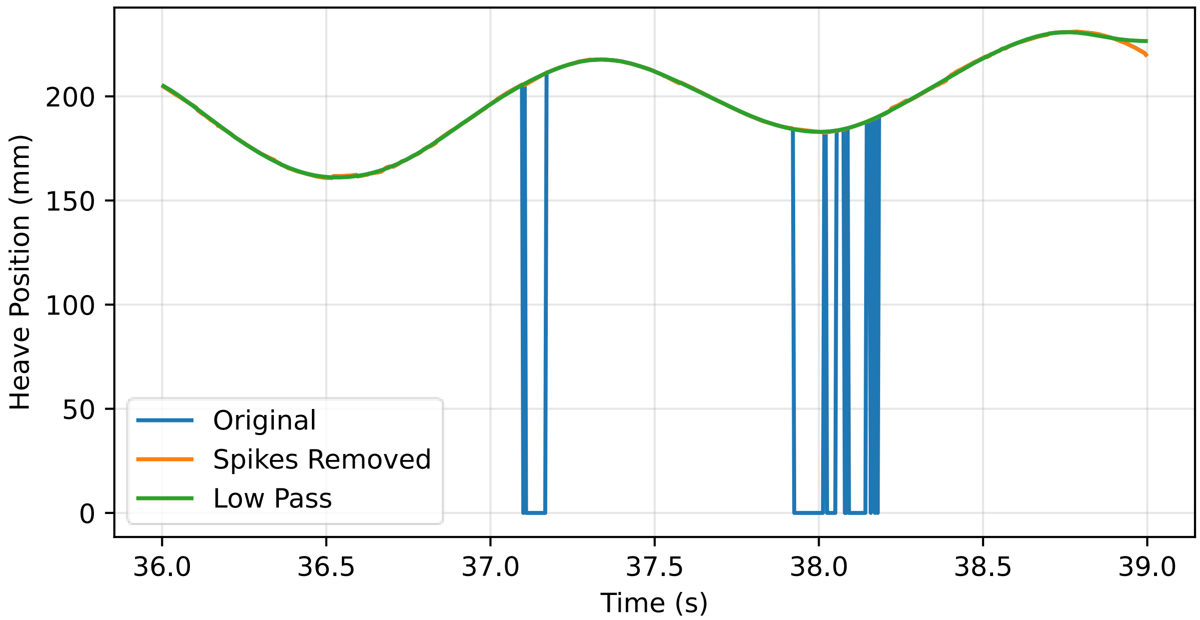

Figure 21. Example of Qualisys motion data filtering and gap filling

From the gap-filled and filtered data, the periodic motion of the device in each DOF was analyzed. The average of the top 10% of amplitudes of the periodic motion was calculated. The amplitude of the periodic motion is defined as the vertical distance between a successive peak and trough. This distinction corrects for the device's drift in the tank. The dominant frequency of the periodic motion was also extracted using a fast Fourier transform. Finally, the maximum displacement of the device from its starting position was calculated.

6.4 Damping Coefficient Processing

The damping coefficient of the PTO system between the heave plate and the float is an important property to understand, as this value is a required input for numerical modeling. The damping coefficient describes the relationship between the force required to move the PTO at a given velocity. The damping coefficient, c_d, is given by Equation (3):

$$c_d = \frac{F_d}{v_{PTO}} \tag{3}$$

where F_d is the damping force in newtons and v_{PTO} is the velocity of the PTO in meters per second.

The PTO velocity was calculated by computing the gradient of the linear potentiometer position over time (shown in green in Figure 22). The force measured by the load cell between the two bodies (shown in blue) is divided by the velocity to compute the damping coefficient (shown in red). The damping coefficient is undefined when the velocity is zero; therefore, the calculation is not considered for the periods that the PTO reaches the end stops of the device and the velocity approaches zero. The average damping coefficient (red dotted line) is then calculated over the duration of the test.

This procedure was repeated eight times for a range of wave heights and periods. The resulting average damping coefficient was found to be 2,473.77 $\frac{Ns}{m}$ with a standard deviation of 84.00 $\frac{Ns}{m}$.

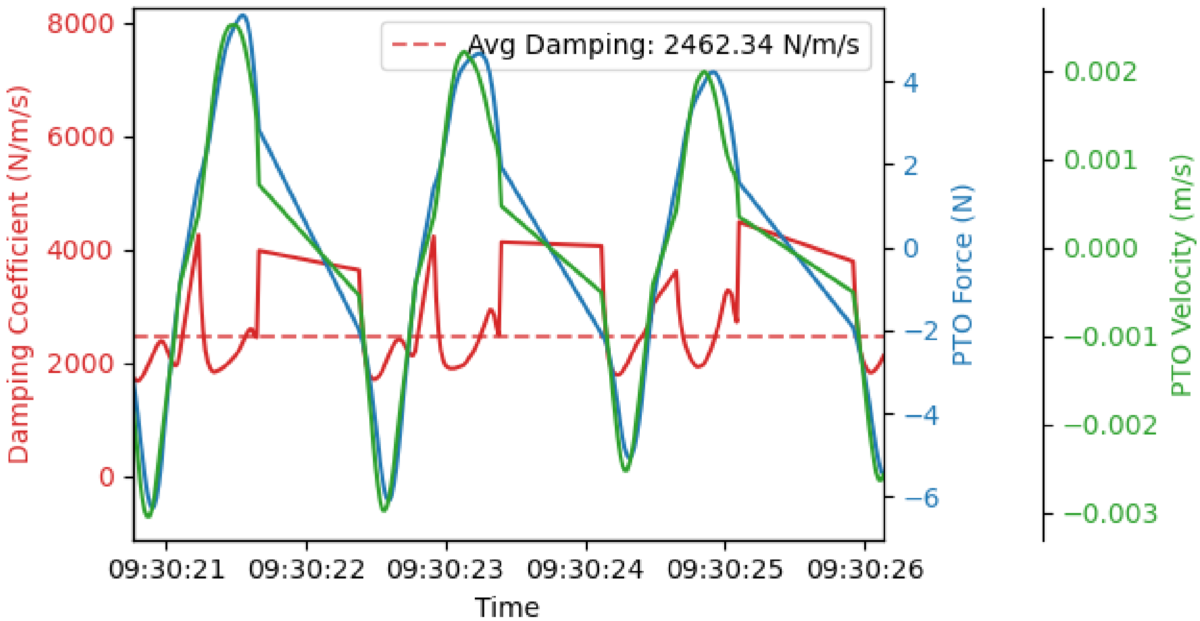

Figure 22. Damping coefficient estimation

7 Experimental Results

7.1 Load Cell Post-Calibration

Scale and offset values for each of the load cells were calculated by computing a linear regression of test weights and measured full-bridge voltage (see section 5.8 for procedures). Figure 23 shows the post-test calibration data (blue) along with the manufacturer's provided calibration (red). Each of the datasets shows a strong linear relationship with coefficients of determination all above 0.999.

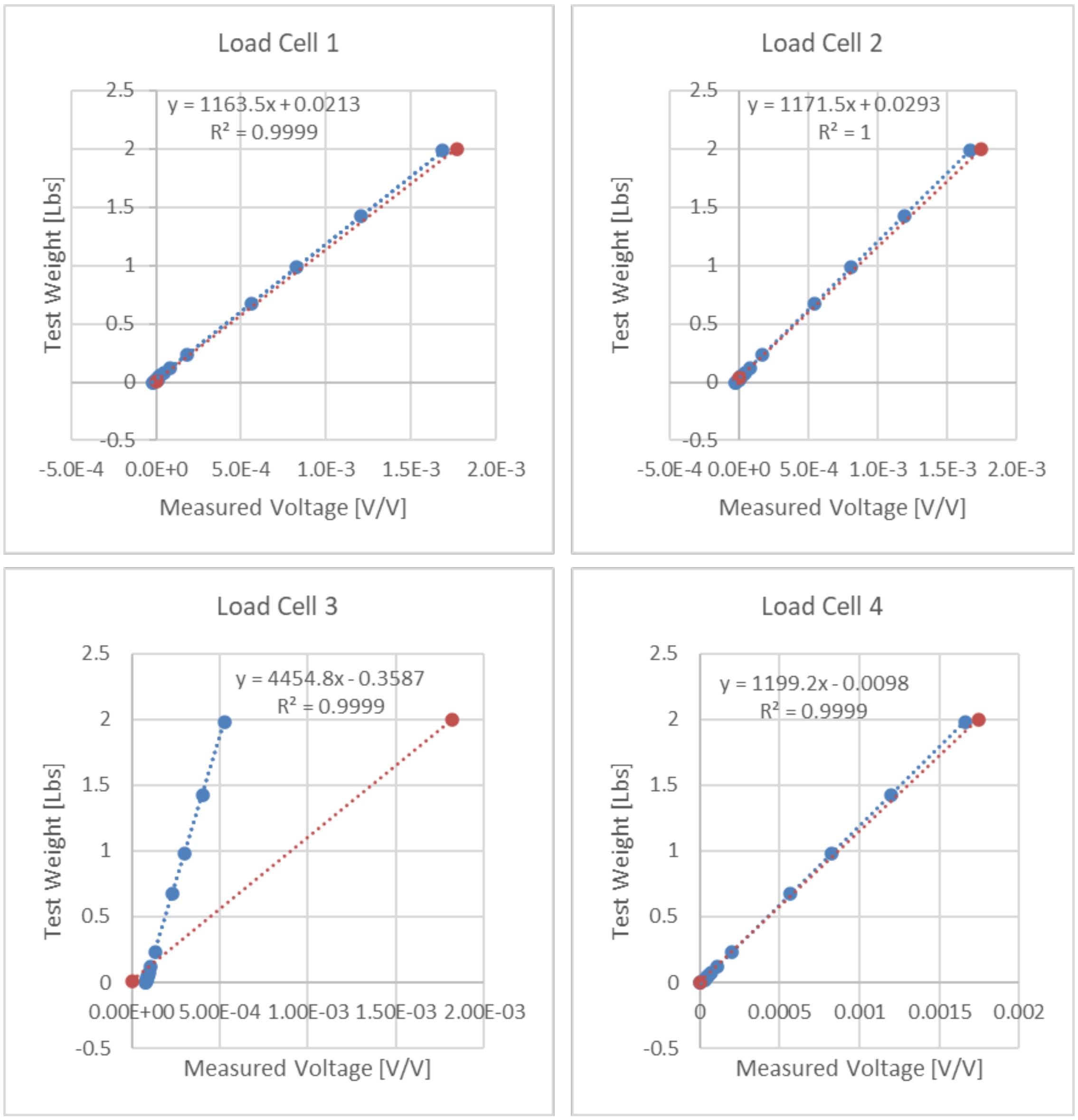

Figure 23. Load cell post-test calibration plots

Table 20 shows the scales and offsets measured in the lab for each load cell along with the scales and offsets supplied by the load cell manufacturer. Each scale parameter measured in the lab (besides LC3) is within 5% of the OEM pre-test calibration value. The difference between the pre- and post-test calibration may be due to a number of factors, including errors in the calibration process or changes in the sensor over the testing period caused by loading, submersion, or temperature changes.

Table 20. Load Cell Calibration Coefficients

Load Cell	Pre-Test OEM Calibration		Post-Test Lab Calibration		%Error
	Scale	Offset	Scale	Offset	Scale
LC1	1,124.67	0.01	1,163.49	0.02	-3.45%
LC2	1,123.22	0.03	1,171.51	0.03	-4.30%
LC3	1,091.64	0.01	4,454.81	-0.36	-308.08%
LC4	1,145.08	0.00	1,199.19	-0.01	-4.73%

The pre-test and post-test calibration values for LC3 vary greatly. This suggests that LC3 was damaged at some point during testing. Through close inspection of the load cell data, it was determined that the damage occurred sometime between the second to last day of testing and the last day of testing and only affected the "Semitaut Polyester w/ Float NLC" case. LC3 data from this case are ignored and LC3 data from other cases should be considered with extra scrutiny.

Lessons Learned

Load Cell Calibration: The load cells should be calibrated in the lab both before and after the tank testing. Because the only in-lab calibration was done after testing, it is uncertain whether the difference in calibration values was due to factors during testing or due to differences in the calibration procedure in the lab versus those used by the OEM. Additionally, the load cells should be calibrated before each day of testing to better inform how the sensor calibration changes throughout testing and alert the operator if a load cell was damaged.

7.2 Tank Characterization Runs

The tank was characterized both with and without the table in place to determine the impact that the table has on the generated wave profile and to determine the actual wave profile that the device would experience when deployed. The surface elevation after the ramp-up period as measured by Wave Gauge 3 for each wave case both with and without the table deployed is plotted in Figure 24. The computed average wave height and period for each case is compiled in Table 21. Wave Gauge 3 is considered because when deployed, the test article is approximately at the position of Wave Gauge 3.

Each wave profile starts with a shift of about 3.5 mm from zero surface elevation followed by small, long-period waves. These waves are from the wave paddle moving from its retracted position to its neutral position. Next, there is an approximately 10-s ramp-up period followed by the test period at the target wave height. Each wave profile begins to show reflections less than 5 s after the ramp-up period ends. The reflections are evident in Figure 24 where the wave heights begin to vary from a relatively constant height. The reflections are most severe for the August mean wave case and least severe for the 50-year extreme case.

The August mean wave case (17.5 mm - 0.9 s) measured waves are slightly larger than the intended size commanded to the controller. At these small wave heights, the wave tank overshoots the commanded wave height; however, the wave period is relatively close to the intended period. The wave heights and periods for the August mean wave cases with and without the table deployed are similar, suggesting that table deployment has little impact on this wave profile.

The December mean wave case (35 mm - 1.1 s) shows good agreement between the intended wave heights and periods and those measured with and without the table. This suggests that the wave tank is tuned to accurately produce these wave sizes when commanded to do so and that the table has little impact on this wave profile.

The 50-year extreme wave case (132 mm - 1.6 s) measured wave heights are smaller than intended and the measured wave periods are shorter than intended. This suggests that at this large wave height the wave tank undershoots the commanded wave height and period. Additionally, the average measured wave height for the 50-year extreme wave case with the table deployed was lower than without the table deployed, and the wave period was similar between the cases. This suggests that for this wave profile the table deployment affects the wave height but not the wave period.

The actual measured wave height and period at Wave Gauge 3 with the table deployed is considered as the actual wave profile for each test case and is reported as the wave height and period for each test in Section 7.3. This value is used rather than the intended wave height and period.

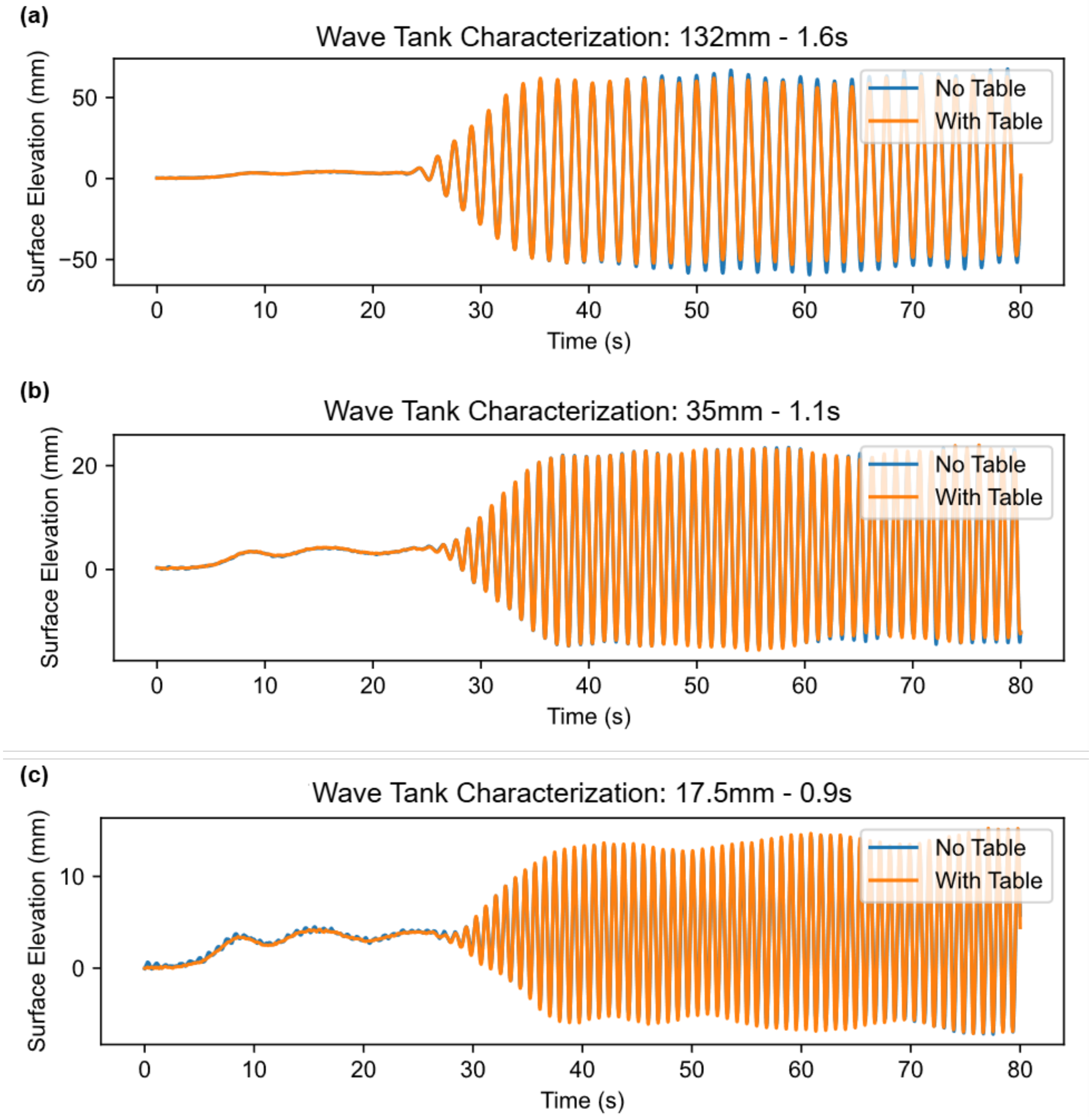

Figure 24. Wave tank characterization with and without the table deployed in the tank. Commanded wave cases: (a) 50-year extreme wave case: 132 mm - 1.6 s, (b) December mean wave case: 35 mm - 1.1 s, and (c) August mean wave case: 17.5 mm - 0.9 s.

Table 21. Wave Tank Characterization Results

Wave Condition	Intended Wave Case		Measured (With Table)		Measured (Without Table)	
	Wave Height	Wave Period	Wave Height	Wave Period	Wave Height	Wave Period
August mean wave at PacWave South (1/100 scale)	17.5 mm	0.9 s	20.4 mm	0.94 s	19.9 mm	0.94 s
December mean wave at PacWave South (1/100 scale)	35 mm	1.1 s	34.5 mm	1.06 s	35.0 mm	1.06 s
Maximum 50-year wave at PacWave South (1/100 scale)	132 mm	1.6 s	114.4 mm	1.23 s	120.0 mm	1.24 s

Lessons Learned

Wave Tank Characterization and Wave Condition Selection: The actual wave height and period incident on the device were different than intended. This means that the intended scaled conditions from the PacWave site were not actually tested. In the future, more work should be done to produce wave profiles closer to the intended test cases, for example, through an iterative process of running waves, processing the results, and changing tank parameters. If the tank is unable to produce the correct wave profile, an alternatively scaled device may be tested so that the wave tank can produce the correct wave profile at the alternative scale.

7.3 Wave Run Results

For each mooring configuration, summary data are presented for the motion of the device and for the mooring line tensions. For the 6-DOF motion data, the periodic displacement range, dominant frequency of motion, and maximum displacement from starting position are presented. Only the position of the float body is considered for the device motion: although the float and heave plate move together, the float body can be better tracked because of the layout of tracking markers on the float. Both the float and heave plate bodies are considered for the PTO motion calculations.

For the mooring line tension data, the neutral tension, maximum tension, average peak tension, and median peak tensions are presented. The reported value is the average of each repetition plus or minus 1 standard deviation of the set of repetitions. Data are presented for each wave height case and each load cell configuration.

One example case is plotted for each mooring configuration. The 114.4 mm - 1.23 s case with both load cells attached was chosen, as it is the most dramatic and highlights interesting results that may be more subtle for the smaller cases. For the motion data, only the position of the float is plotted.

7.3.1 Catenary Chain Configuration

Table 22. 6-DOF Motion Average Computed Values for Catenary Chain Configuration Float Body

Linear displacement values reported in mm. Angular displacement values reported in deg. Frequency values reported in Hz. Format: mean ± standard deviation. FH = free-hanging; Sec = secured; No LC = no load cell.

		114.4 mm - 1.23 s			34.5 mm - 1.06 s			20.4 mm - 0.94 s		
		FH LC	Sec LC	No LC	FH LC	Sec LC	No LC	FH LC	Sec LC	No LC
Periodic Displacement Range	Surge [mm]	20.7 ± 0.6	20.1 ± 0.7	24.8 ± 0.5	21.1 ± 0.2	23.1 ± 0.3	27.7 ± 1.4	12.6 ± 0.1	11.8 ± 0.4	13.4 ± 0.1
	Sway [mm]	5.4 ± 0.4	6.2 ± 0.6	7.3 ± 0.6	2.6 ± 0.2	6.4 ± 0.3	6.8 ± 0.6	2.7 ± 0.1	0.9 ± 0.0	1.3 ± 0.9
	Heave [mm]	31.7 ± 1.3	32.4 ± 1.4	12.9 ± 1.9	8.7 ± 0.1	8.1 ± 0.5	8.8 ± 0.3	2.0 ± 0.0	1.6 ± 0.2	1.9 ± 0.3
	Roll [deg]	0.6 ± 0.1	0.7 ± 0.1	0.8 ± 0.2	0.2 ± 0.0	0.6 ± 0.1	0.6 ± 0.3	0.2 ± 0.0	0.2 ± 0.1	0.1 ± 0.1
	Pitch [deg]	1.4 ± 0.1	1.4 ± 0.3	1.5 ± 0.1	1.2 ± 0.0	1.4 ± 0.0	1.7 ± 0.1	0.9 ± 0.0	0.9 ± 0.2	0.9 ± 0.1
	Yaw [deg]	1.2 ± 0.2	1.3 ± 0.2	0.8 ± 0.1	0.2 ± 0.0	0.2 ± 0.0	0.7 ± 0.1	0.1 ± 0.0	0.1 ± 0.0	0.2 ± 0.0
	PTO [mm]	62.2 ± 4.0	81.2 ± 38.7	59.9 ± 0.9	-	-	-	-	-	-
Dominant Frequency of Motion	Surge [s]	0.6 ± 0.0	0.5 ± 0.2	0.6 ± 0.0	0.9 ± 0.0	0.9 ± 0.0	0.9 ± 0.0	1.1 ± 0.0	1.1 ± 0.0	1.1 ± 0.0
	Sway [s]	0.4 ± 0.2	0.5 ± 0.2	0.5 ± 0.2	0.7 ± 0.4	0.2 ± 0.1	0.2 ± 0.0	0.8 ± 0.5	0.8 ± 0.5	0.5 ± 0.5
	Heave [s]	0.6 ± 0.0	0.6 ± 0.0	0.6 ± 0.0	0.9 ± 0.0	0.9 ± 0.0	0.9 ± 0.0	1.1 ± 0.0	1.1 ± 0.0	1.1 ± 0.0
	Roll [s]	0.3 ± 0.0	0.4 ± 0.2	0.3 ± 0.0	0.3 ± 0.0	0.7 ± 0.3	0.9 ± 0.0	1.1 ± 0.0	1.1 ± 0.0	1.1 ± 0.0
	Pitch [s]	0.3 ± 0.0	0.3 ± 0.0	0.3 ± 0.0	0.9 ± 0.0	0.9 ± 0.0	0.9 ± 0.0	1.1 ± 0.0	1.1 ± 0.0	1.1 ± 0.0
	Yaw [s]	0.2 ± 0.0	0.3 ± 0.0	0.3 ± 0.0	0.3 ± 0.0	0.2 ± 0.0	0.2 ± 0.0	0.2 ± 0.0	0.2 ± 0.0	0.3 ± 0.1
	PTO [s]	0.3 ± 0.0	0.3 ± 0.3	0.5 ± 0.2	-	-	-	-	-	-
Max Displacement	Surge [mm]	385.7 ± 30.3	311.1 ± 28.2	404.9 ± 12.9	289.9 ± 4.9	260.1 ± 16.2	315.5 ± 3.4	155.2 ± 8.0	96.0 ± 10.2	177.4 ± 6.9
	Sway [mm]	83.8 ± 87.3	106.8 ± 98.6	321.1 ± 14.5	105.1 ± 23.4	114.6 ± 185.1	211.3 ± 343.5	50.2 ± 5.8	12.2 ± 10.5	67.3 ± 87.7
	Heave [mm]	64.6 ± 2.9	59.1 ± 1.5	56.1 ± 1.3	8.4 ± 0.2	7.4 ± 1.1	8.2 ± 0.7	4.5 ± 0.2	2.6 ± 1.6	5.0 ± 0.0
	Roll [deg]	3.7 ± 1.3	3.4 ± 1.5	2.5 ± 1.3	0.5 ± 0.1	2.7 ± 0.4	1.4 ± 0.6	0.3 ± 0.1	0.4 ± 0.0	0.2 ± 0.1
	Pitch [deg]	9.7 ± 0.5	7.7 ± 2.5	6.1 ± 0.1	2.6 ± 0.1	2.0 ± 0.2	2.5 ± 1.2	1.3 ± 0.1	0.8 ± 0.2	1.3 ± 0.1
	Yaw [deg]	31.1 ± 12.3	21.3 ± 25.0	4.7 ± 6.2	31.9 ± 6.8	9.5 ± 7.3	8.8 ± 3.7	25.6 ± 0.8	8.7 ± 2.0	3.1 ± 1.1
	PTO [mm]	3.2 ± 1.3	2.1 ± 2.1	2.0 ± 0.8	-	-	-	-	-	-

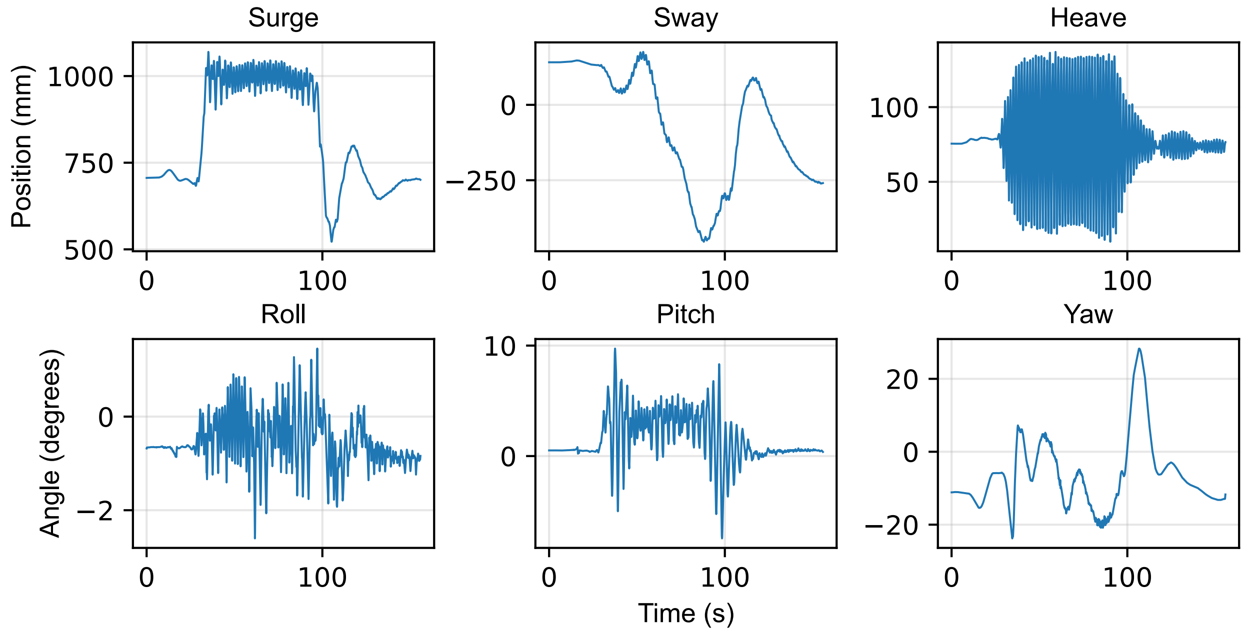

Figure 25. Plot of 6-DOF motion for the catenary chain configuration with WEC load cells attached subjected to the 114.4 mm - 1.23 s wave case

Table 23. Mooring Line Tension Values for Catenary Chain Configuration

Format: mean ± standard deviation

		114.4 mm - 1.23 s			34.5 mm - 1.06 s			20.4 mm - 0.94 s		
		FH LC	**Sec LC**	**No LC**	**FH LC**	**Sec LC**	**No LC**	**FH LC**	**Sec LC**	**No LC**
Neutral tension [N]	**WEC**	1.0E-1 ± 8.9E-3	1.1E-1 ± 8.0E-3	-	9.6E-2 ± 8.8E-4	1.1E-1 ± 3.1E-3	-	1.0E-1 ± 2.9E-3	1.1E-1 ± 7.1E-4	-
	Anchor	8.9E-2 ± 2.6E-3	6.3E-2 ± 4.6E-2	1.5E-1 ± 1.6E-2	8.6E-2 ± 6.4E-3	1.1E-1 ± 2.8E-2	1.0E-1 ± 1.2E-2	8.8E-2 ± 5.5E-3	7.5E-2 ± 9.6E-3	7.2E-2 ± 2.8E-4
Maximum tension [N]	**WEC**	2.7E+0 ± 5.3E-1	1.9E+0 ± 3.9E-1	-	3.3E-1 ± 2.4E-2	3.5E-1 ± 8.7E-2	-	1.2E-1 ± 1.8E-3	1.2E-1 ± 4.8E-4	-
	Anchor	2.6E+0 ± 5.5E-1	1.8E+0 ± 4.1E-1	3.1E+0 ± 4.7E-1	2.4E-1 ± 1.7E-2	2.6E-1 ± 8.0E-2	3.1E-1 ± 1.6E-2	9.7E-2 ± 8.1E-3	8.0E-2 ± 1.1E-2	1.0E-1 ± 3.9E-3
Average periodic peak tension [N]	**WEC**	4.1E-1 ± 2.6E-2	4.5E-1 ± 6.2E-2	-	1.9E-1 ± 4.9E-3	1.5E-1 ± 1.3E-2	-	1.1E-1 ± 2.8E-3	1.1E-1 ± 5.2E-4	-
	Anchor	3.6E-1 ± 2.8E-2	3.8E-1 ± 5.6E-2	4.0E-1 ± 3.3E-2	1.5E-1 ± 4.0E-3	1.1E-1 ± 1.2E-2	1.2E-1 ± 6.4E-3	7.8E-2 ± 2.1E-3	5.4E-2 ± 3.6E-3	7.7E-2 ± 3.0E-3
Maximum tension relative to neutral tension [N]	**WEC**	2.6E+0 ± 5.3E-1	1.8E+0 ± 3.8E-1	-	2.4E-1 ± 2.4E-2	2.4E-1 ± 8.9E-2	-	1.7E-2 ± 1.8E-3	1.7E-2 ± 7.6E-4	-
	Anchor	2.6E+0 ± 5.5E-1	1.8E+0 ± 3.6E-1	3.0E+0 ± 4.9E-1	1.5E-1 ± 2.3E-2	1.5E-1 ± 1.0E-1	2.1E-1 ± 2.6E-2	9.8E-3 ± 8.0E-3	5.5E-3 ± 2.4E-3	2.9E-2 ± 3.7E-3
Rise time from neutral tension to initial maximum [s]	**Anchor**	1.957 ± 0.095	1.777 ± 0.078	1.788 ± 0.065	-	-	-	-	-	-

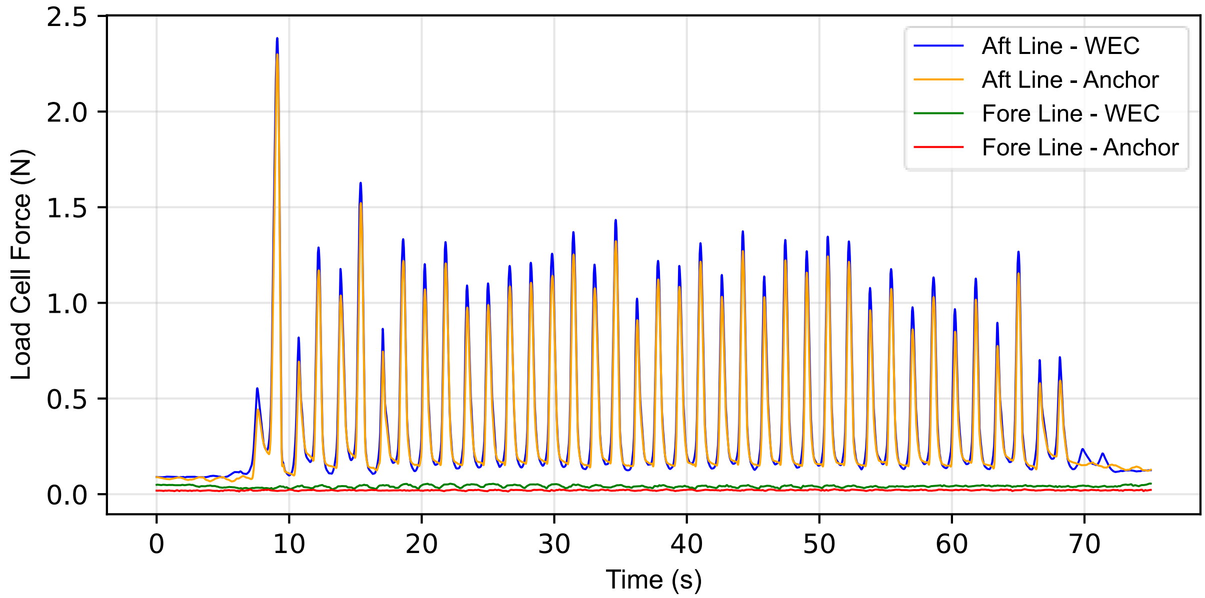

Figure 26. Plot of mooring loads for the catenary chain configuration with WEC load cells attached subjected to 114.4 mm - 1.23 s wave case

7.3.2 Taut Nylon Configuration

Table 24. 6-DOF Motion Average Computed Values for Taut Nylon Configuration Float Body

Format: mean ± standard deviation

		114.4 mm - 1.23 s		34.5 mm - 1.06 s		20.4 mm - 0.94 s	
		FH LC	**No LC**	**FH LC**	**No LC**	**FH LC**	**No LC**
Periodic Displacement Range	**Surge [mm]**	18.9 ± 3.8	22.3 ± 1.7	24.6 ± 0.2	27.2 ± 0.2	12.0 ± 0.0	13.8 ± 0.2
	Sway [mm]	6.8 ± 1.9	7.1 ± 1.1	3.4 ± 0.2	4.4 ± 0.2	2.3 ± 1.0	1.9 ± 0.1
	Heave [mm]	26.1 ± 6.5	14.6 ± 0.9	8.6 ± 0.7	8.5 ± 0.1	2.0 ± 0.3	2.0 ± 0.1
	Roll [deg]	0.8 ± 0.1	1.0 ± 0.2	0.3 ± 0.1	1.1 ± 0.0	0.2 ± 0.1	1.1 ± 0.1
	Pitch [deg]	1.5 ± 0.3	1.5 ± 0.1	1.5 ± 0.1	1.5 ± 0.1	0.8 ± 0.0	0.8 ± 0.0
	Yaw [deg]	0.7 ± 0.2	0.9 ± 0.0	0.2 ± 0.1	1.3 ± 0.1	0.1 ± 0.0	0.6 ± 0.0
	PTO [mm]	71.3 ± 10.2	62.8 ± 3.2	-	-	-	-
Dominant Frequency [Hz] of Motion	**Surge [Hz]**	0.62 ± 0.00	0.63 ± 0.00	0.91 ± 0.00	0.91 ± 0.00	1.11 ± 0.00	1.11 ± 0.00
	Sway [Hz]	0.35 ± 0.24	0.4 ± 0.18	0.2 ± 0.00	0.5 ± 0.37	0.2 ± 0.00	0.8 ± 0.53
	Heave [Hz]	0.62 ± 0.00	0.6 ± 0.00	0.9 ± 0.00	0.9 ± 0.00	1.1 ± 0.00	1.1 ± 0.00
	Roll [Hz]	0.38 ± 0.21	0.4 ± 0.18	0.9 ± 0.00	0.5 ± 0.34	1.1 ± 0.00	1.1 ± 0.01
	Pitch [Hz]	0.41 ± 0.18	0.3 ± 0.00	0.9 ± 0.00	0.9 ± 0.00	1.1 ± 0.00	1.1 ± 0.00
	Yaw [Hz]	0.24 ± 0.06	0.3 ± 0.01	0.2 ± 0.07	0.4 ± 0.30	0.2 ± 0.00	0.6 ± 0.54
	PTO [Hz]	0.52 ± 0.19	0.3 ± 0.01	-	-	-	-
Max Displacement	**Surge [mm]**	540.7 ± 29.5	379.8 ± 16.9	132.1 ± 37.2	68.5 ± 0.2	51.5 ± 6.6	30.8 ± 0.6
	Sway [mm]	219.5 ± 196.6	32.7 ± 28.5	453.6 ± 107.7	488.2 ± 6.6	92.3 ± 19.0	32.6 ± 6.3
	Heave[mm]	50.0 ± 16.5	61.4 ± 17.7	9.4 ± 0.2	10.0 ± 0.3	2.0 ± 0.2	4.2 ± 0.0
	Roll [deg]	2.4 ± 0.7	3.3 ± 0.8	0.6 ± 0.3	1.4 ± 0.3	0.2 ± 0.2	1.6 ± 0.1
	Pitch [deg]	8.4 ± 0.6	8.4 ± 1.2	1.6 ± 0.2	2.2 ± 0.1	0.7 ± 0.1	1.5 ± 0.1
	Yaw [deg]	46.1 ± 45.3	6.3 ± 1.8	29.7 ± 14.6	2.4 ± 0.1	21.5 ± 6.7	1.2 ± 0.1
	PTO [mm]	3.9 ± 2.0	3.1 ± 0.7	-	-	-	-

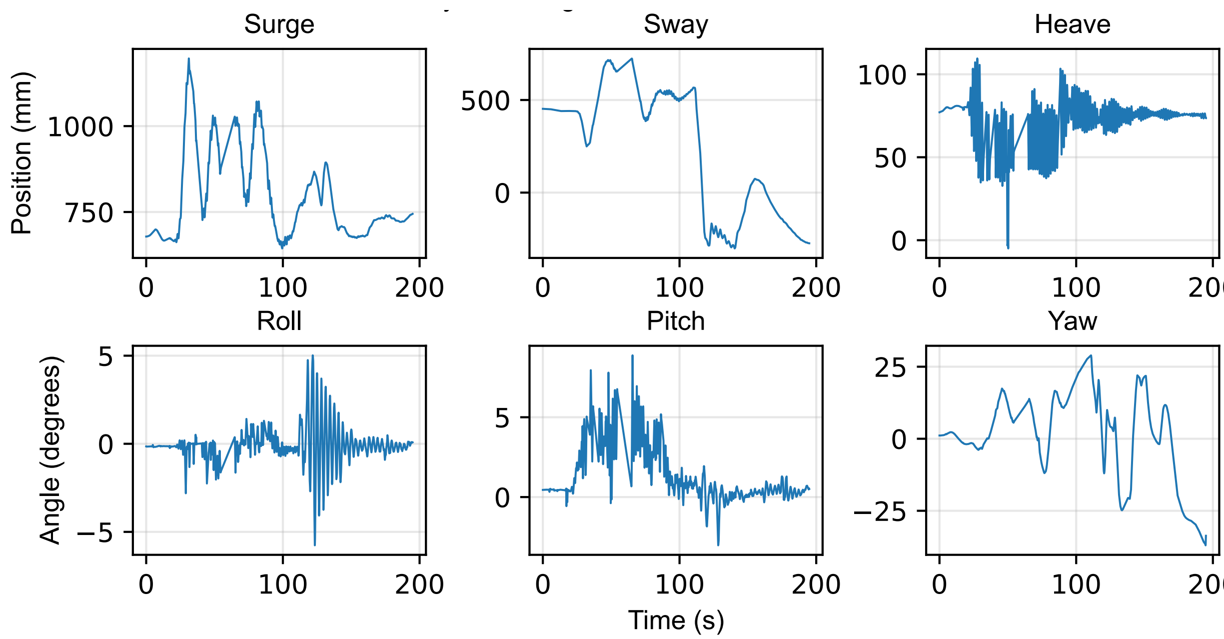

Figure 27. Plot of 6-DOF motion for the taut nylon configuration with WEC load cells attached subjected to the 114.4 mm - 1.23 s wave case

Table 25. Mooring Line Tension Values for Taut Nylon Configuration

Format: mean ± standard deviation

		114.4 mm - 1.23 s		34.5 mm - 1.06 s		20.4 mm - 0.94 s	
		FH LC	**No LC**	**FH LC**	**No LC**	**FH LC**	**No LC**
Neutral tension [N]	**WEC**	7.3E-2 ± 9.5E-3	-	6.3E-2 ± 2.7E-3	-	6.1E-2 ± 3.6E-3	-
	Anchor	1.6E-2 ± 1.7E-3	1.3E-1 ± 1.2E-2	1.5E-2 ± 2.3E-3	1.3E-1 ± 8.3E-4	1.5E-2 ± 1.5E-3	1.3E-1 ± 1.6E-3
Maximum tension [N]	**WEC**	6.2E-1 ± 3.7E-2	-	1.5E-1 ± 2.0E-2	-	8.5E-2 ± 1.5E-3	-
	Anchor	5.7E-1 ± 3.5E-2	5.7E-1 ± 1.8E-2	1.1E-1 ± 1.6E-2	2.0E-1 ± 4.8E-3	5.1E-2 ± 1.8E-3	1.7E-1 ± 8.2E-4
Average periodic peak tension [N]	**WEC**	3.1E-1 ± 1.2E-1	-	7.6E-2 ± 1.7E-2	-	6.4E-2 ± 2.1E-3	-
	Anchor	2.6E-1 ± 1.2E-1	3.7E-1 ± 1.9E-2	3.2E-2 ± 1.5E-2	1.4E-1 ± 1.2E-3	2.9E-2 ± 1.8E-3	1.4E-1 ± 1.4E-3
Maximum tension relative to neutral tension [N]	**WEC**	5.4E-1 ± 2.8E-2	-	9.1E-2 ± 1.8E-2	-	2.4E-2 ± 4.9E-3	-
	Anchor	5.5E-1 ± 3.5E-2	4.4E-1 ± 1.3E-2	9.4E-2 ± 1.5E-2	7.9E-2 ± 4.1E-3	3.5E-2 ± 3.1E-3	4.1E-2 ± 2.4E-3
Rise time from neutral tension to initial maximum [s]	**Anchor**	7.356 ± 0.098	14.572 ± 0.874				

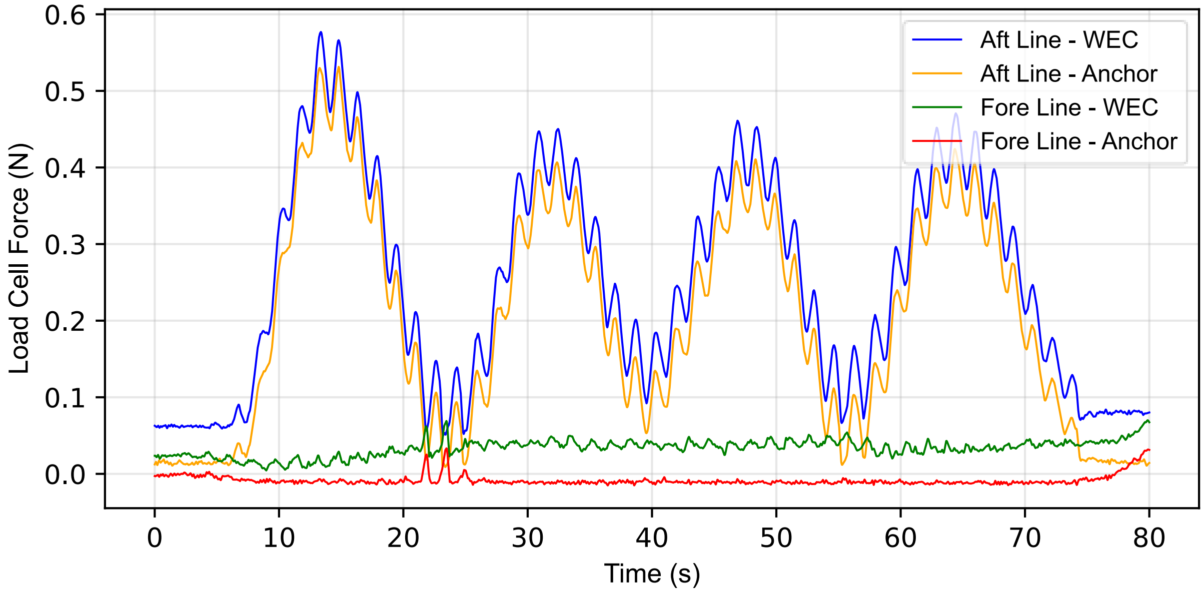

Figure 28. Plot of mooring loads for the taut nylon configuration with WEC load cells attached subjected to the 114.4 mm - 1.23 s wave case

7.3.3 Semitaut Nylon Configuration

Table 26. 6-DOF Motion Average Computed Values for Semitaut Nylon Configuration Float Body

Format: mean ± standard deviation

		114.4 mm - 1.23 s		34.5 mm - 1.06 s		20.4 mm - 0.94 s	
		FH LC	No LC	FH LC	No LC	FH LC	No LC
Periodic Displacement Range	Surge [mm]	19.1 ± 1.3	21.2 ± 0.5	24.1 ± 0.5	27.0 ± 0.7	12.3 ± 0.0	15.2 ± 0.1
	Sway [mm]	5.5 ± 0.8	6.3 ± 1.0	6.0 ± 0.3	3.9 ± 0.7	1.2 ± 0.4	1.1 ± 0.4
	Heave [mm]	32.5 ± 0.4	15.5 ± 0.8	7.3 ± 1.5	8.4 ± 1.2	1.7 ± 0.0	1.7 ± 0.0
	Roll [Deg]	0.6 ± 0.1	0.8 ± 0.1	0.4 ± 0.0	0.5 ± 0.1	0.1 ± 0.0	0.4 ± 0.1
	Pitch [Deg]	1.3 ± 0.1	1.4 ± 0.1	1.4 ± 0.0	1.7 ± 0.0	0.9 ± 0.0	1.1 ± 0.0
	Yaw [Deg]	1.3 ± 0.1	1.1 ± 0.4	0.3 ± 0.1	0.6 ± 0.0	0.1 ± 0.0	0.3 ± 0.0
	PTO [mm]	59.1 ± 0.3	65.9 ± 7.7	-	-	-	-
Dominant Frequency of Motion	Surge [Hz]	0.63 ± 0.00	0.62 ± 0.00	0.91 ± 0.00	0.91 ± 0.00	1.11 ± 0.00	1.11 ± 0.00
	Sway [Hz]	0.52 ± 0.19	0.43 ± 0.22	0.67 ± 0.40	0.21 ± 0.01	0.20 ± 0.00	0.21 ± 0.01
	Heave [Hz]	0.62 ± 0.00	0.62 ± 0.00	0.91 ± 0.00	0.91 ± 0.01	1.11 ± 0.01	1.11 ± 0.00
	Roll [Hz]	0.52 ± 0.19	0.37 ± 0.17	0.71 ± 0.34	0.61 ± 0.42	1.11 ± 0.01	0.24 ± 0.02
	Pitch [Hz]	0.31 ± 0.01	0.30 ± 0.01	0.71 ± 0.34	0.91 ± 0.00	1.11 ± 0.00	1.11 ± 0.00
	Yaw [Hz]	0.26 ± 0.05	0.28 ± 0.05	0.21 ± 0.00	0.24 ± 0.03	0.21 ± 0.01	0.26 ± 0.07
	PTO [Hz]	0.53 ± 0.18	0.38 ± 0.17	-	-	-	-
Max Displacement	Surge [mm]	362.3 ± 15.0	458.9 ± 35.6	158.1 ± 33.4	236.4 ± 11.8	76.0 ± 16.7	148.9 ± 2.4
	Sway [mm]	193.4 ± 217.0	328.7 ± 410.7	18.6 ± 14.7	417.6 ± 589.7	85.1 ± 49.3	43.0 ± 21.9
	Heave [mm]	60.5 ± 1.3	45.6 ± 12.6	5.9 ± 2.4	6.9 ± 1.4	4.5 ± 0.1	4.6 ± 0.1
	Roll [Deg]	2.2 ± 0.4	3.3 ± 1.0	1.7 ± 0.2	1.1 ± 0.8	0.2 ± 0.1	1.0 ± 0.1
	Pitch [Deg]	9.1 ± 1.5	7.6 ± 2.0	2.2 ± 0.6	2.5 ± 1.4	0.8 ± 0.2	1.1 ± 0.1
	Yaw [Deg]	29.3 ± 10.7	9.1 ± 7.9	9.1 ± 14.1	16.2 ± 2.4	18.1 ± 7.5	4.3 ± 0.9
	PTO [mm]	2.2 ± 0.4	3.2 ± 1.1	-	-	-	-

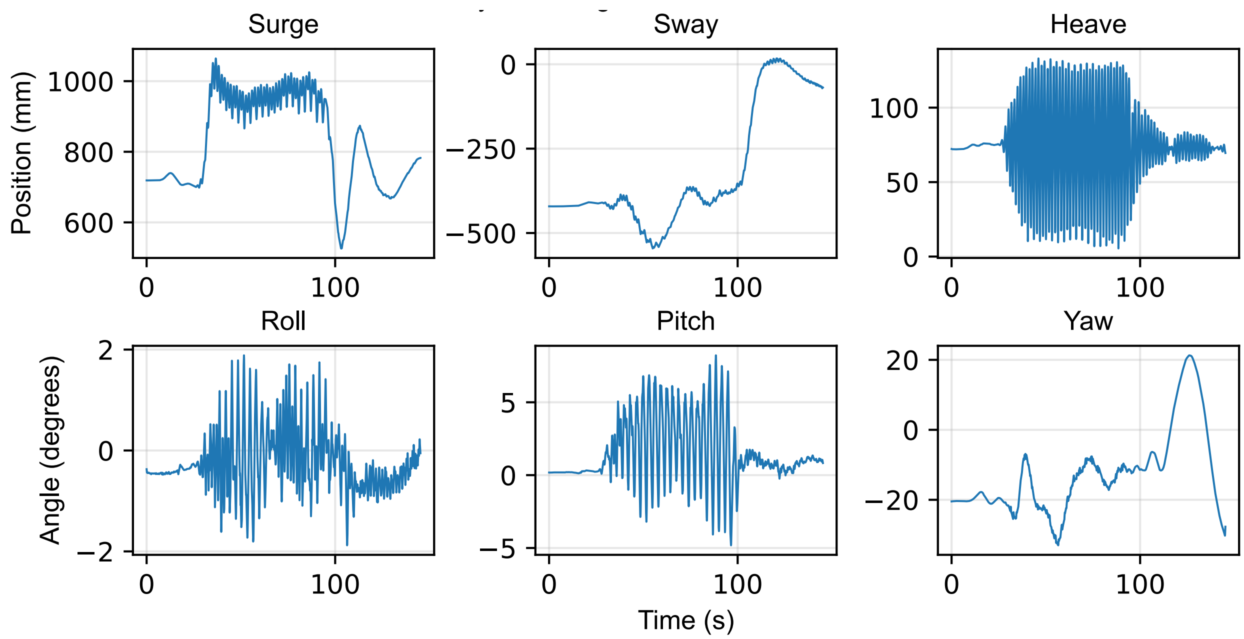

Figure 29. Plot of 6-DOF motion for the semitaut nylon configuration with WEC load cells attached subjected to the 114.4 mm - 1.23 s wave case

Table 27. Mooring Line Tension Values for Semitaut Nylon Configuration

Format: mean ± standard deviation

		114.4 mm - 1.23 s		34.5 mm - 1.06 s		20.4 mm - 0.94 s	
		FH LC	**No LC**	**FH LC**	**No LC**	**FH LC**	**No LC**
Neutral tension [N]	**WEC**	9.6E-2 ± 1.7E-2	-	7.2E-2 ± 4.5E-3	-	6.7E-2 ± 4.7E-4	-
	Anchor	5.4E-2 ± 2.0E-3	6.0E-2 ± 5.4E-3	5.0E-2 ± 3.9E-3	5.5E-2 ± 8.4E-4	4.9E-2 ± 5.5E-3	5.2E-2 ± 2.9E-3
Maximum tension [N]	**WEC**	6.5E-1 ± 6.5E-2	-	1.7E-1 ± 4.6E-2	-	8.7E-2 ± 1.4E-2	-
	Anchor	5.8E-1 ± 4.4E-2	7.7E-1 ± 3.5E-2	1.2E-1 ± 4.9E-2	2.0E-1 ± 5.0E-2	6.6E-2 ± 3.4E-3	7.5E-2 ± 1.6E-3
Average periodic peak tension [N]	**WEC**	3.7E-1 ± 1.5E-2	-	9.5E-2 ± 1.4E-2	-	7.1E-2 ± 4.2E-4	-
	Anchor	3.1E-1 ± 1.5E-3	3.1E-1 ± 6.5E-2	6.8E-2 ± 1.6E-2	7.9E-2 ± 2.3E-2	4.9E-2 ± 6.6E-4	5.4E-2 ± 2.3E-4
Maximum tension relative to neutral tension [N]	**WEC**	5.5E-1 ± 4.9E-2	-	9.8E-2 ± 5.0E-2	-	2.0E-2 ± 1.4E-2	-
	Anchor	5.2E-1 ± 4.2E-2	7.1E-1 ± 3.1E-2	7.2E-2 ± 5.2E-2	1.4E-1 ± 5.0E-2	1.7E-2 ± 2.8E-3	2.3E-2 ± 4.2E-3
Rise time from neutral tension to initial maximum [s]	**Anchor**	5.829 ± 0.925	5.012 ± 0.057				

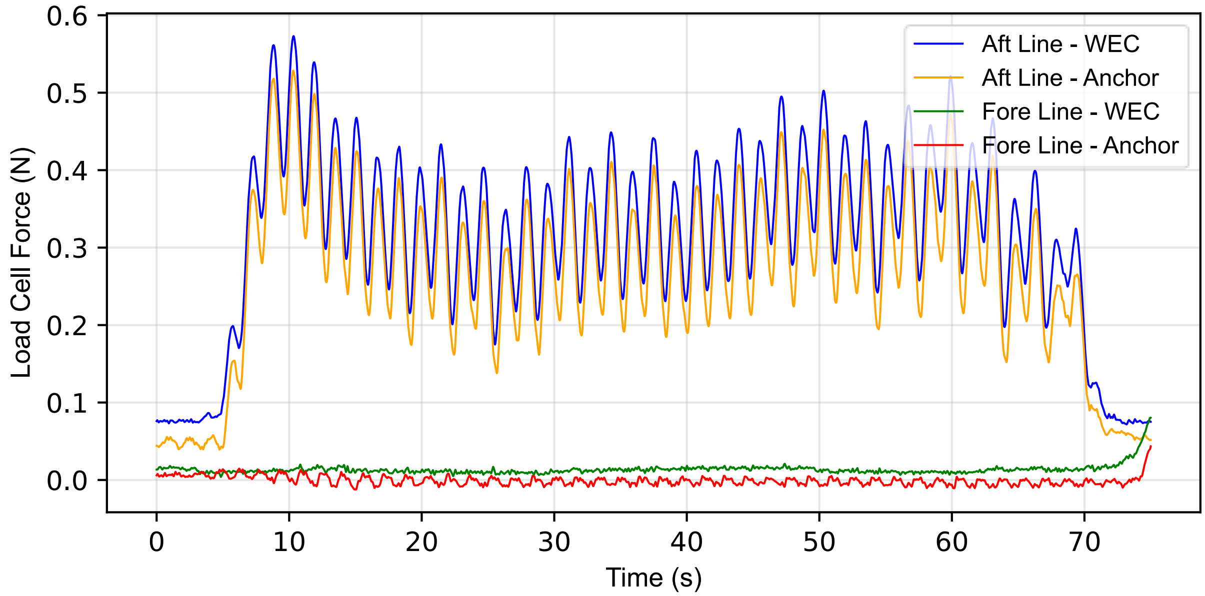

Figure 30. Plot of mooring loads for the semitaut nylon configuration with WEC load cells attached subjected to the 114.4 mm - 1.23 s wave case

7.3.4 Semitaut Polyester Configuration

Table 28. 6-DOF Motion Average Computed Values for Semitaut Polyester Configuration

Format: mean ± standard deviation

		114.4 mm - 1.23 s		34.5 mm - 1.06 s		20.4 mm - 0.94 s	
		FH LC	**No LC**	**FH LC**	**No LC**	**FH LC**	**No LC**
Periodic Displacement Range	**Surge [mm]**	28.8 ± 1.4	26.7 ± 0.6	23.5 ± 0.4	27.3 ± 1.8	14.8 ± 0.0	13.8 ± 0.2
	Sway [mm]	6.7 ± 0.9	6.2 ± 0.3	2.5 ± 0.8	4.1 ± 0.4	1.1 ± 0.1	1.0 ± 0.1
	Heave [mm]	28.1 ± 1.3	17.0 ± 0.1	7.6 ± 0.0	7.3 ± 1.4	1.8 ± 0.0	1.9 ± 0.0
	Roll [deg]	3.9 ± 5.0	1.1 ± 0.1	0.2 ± 0.1	0.8 ± 0.1	0.1 ± 0.0	0.3 ± 0.0
	Pitch [deg]	2.1 ± 0.3	1.9 ± 0.0	1.5 ± 0.0	1.7 ± 0.1	1.0 ± 0.0	1.1 ± 0.1
	Yaw [deg]	2.5 ± 2.3	1.4 ± 0.0	0.1 ± 0.0	1.4 ± 0.7	0.1 ± 0.0	0.4 ± 0.1
	PTO [mm]	94.0 ± 6.4	58.2 ± 0.9	-	-	-	-
Dominant Frequency of Motion	**Surge [Hz]**	0.62 ± 0.00	0.62 ± 0.00	0.91 ± 0.00	0.91 ± 0.00	1.11 ± 0.00	1.11 ± 0.00
	Sway [Hz]	0.62 ± 0.01	0.31 ± 0.01	0.44 ± 0.40	0.56 ± 0.50	0.51 ± 0.52	0.50 ± 0.52
	Heave [Hz]	0.62 ± 0.00	0.62 ± 0.00	0.91 ± 0.00	0.91 ± 0.00	1.11 ± 0.00	1.11 ± 0.00
	Roll [Hz]	0.27 ± 0.05	0.31 ± 0.00	0.33 ± 0.01	0.60 ± 0.42	1.11 ± 0.00	0.24 ± 0.02
	Pitch [Hz]	0.31 ± 0.02	0.30 ± 0.01	0.52 ± 0.34	0.32 ± 0.00	1.11 ± 0.00	1.11 ± 0.00
	Yaw [Hz]	0.21 ± 0.00	0.26 ± 0.07	0.21 ± 0.00	0.23 ± 0.02	0.21 ± 0.00	0.22 ± 0.02
	PTO [Hz]	0.32 ± 0.01	0.31 ± 0.00	-	-	-	-
Max Displacement	**Surge [mm]**	378.7 ± 24.3	415.0 ± 0.5	289.6 ± 12.2	290.5 ± 54.4	158.9 ± 16.5	209.0 ± 3.4
	Sway [mm]	84.9 ± 93.8	74.6 ± 47.1	72.8 ± 98.6	324.9 ± 419.2	41.5 ± 14.7	42.6 ± 31.2
	Heave [mm]	51.8 ± 2.7	58.4 ± 22.7	8.8 ± 1.3	9.0 ± 0.8	4.7 ± 0.1	4.8 ± 0.4
	Roll [deg]	49.0 ± 80.2	4.2 ± 1.8	0.9 ± 0.7	1.4 ± 0.2	0.1 ± 0.0	0.6 ± 0.3
	Pitch [deg]	12.1 ± 4.3	8.7 ± 0.2	3.1 ± 1.0	4.0 ± 1.0	0.7 ± 0.0	1.1 ± 0.1
	Yaw [deg]	123.5 ± 49.0	6.0 ± 8.0	57.8 ± 20.2	2.6 ± 1.8	41.8 ± 8.4	0.2 ± 0.2
	PTO [mm]	4.4 ± 1.0	3.7 ± 0.7		-	-	-

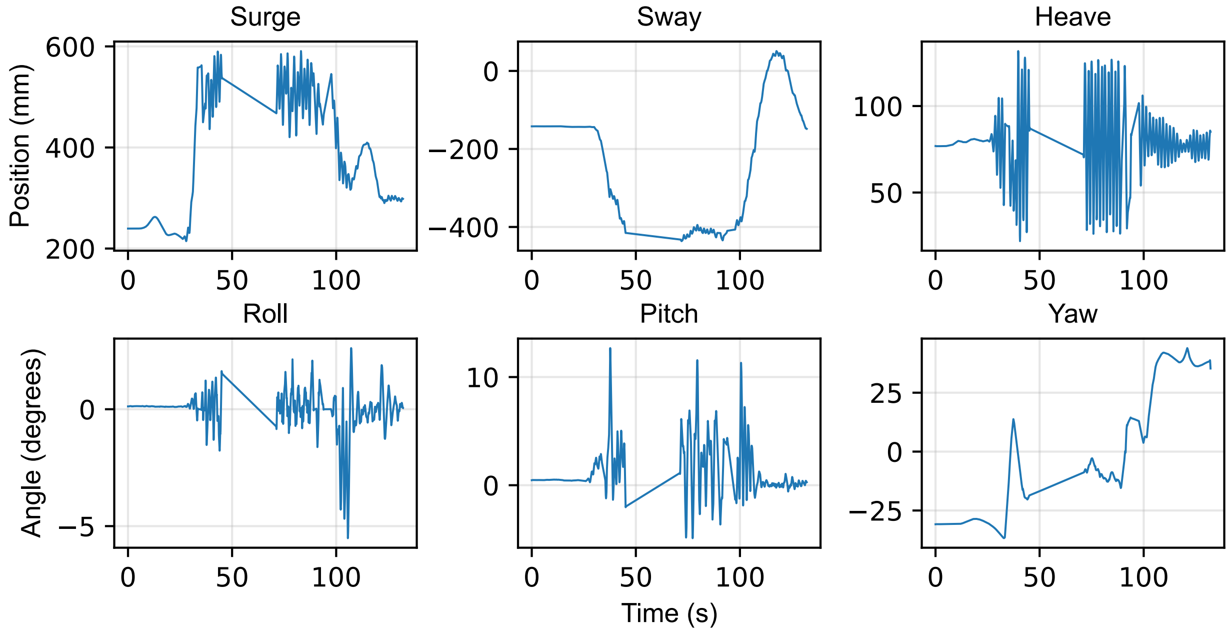

Figure 31. Plot of 6-DOF motion for the semitaut polyester configuration with WEC load cells attached subjected to the 114.4 mm - 1.23 s wave case

Table 29. Mooring Line Tension Values for Semitaut Polyester Configuration

Format: mean ± standard deviation

		114.4 mm - 1.23 s		34.5 mm - 1.06 s		20.4 mm - 0.94 s	
		FH LC	No LC	FH LC	No LC	FH LC	No LC
Neutral tension [N]	**WEC**	1.0E-1 ± 5.6E-3		1.1E-1 ± 1.8E-3		1.1E-1 ± 2.1E-4	
	Anchor	1.1E-1 ± 4.9E-2		1.1E-1 ± 3.5E-2		7.7E-2 ± 2.7E-3	
Maximum tension [N]	**WEC**	3.5E+0 ± 6.2E-1		3.3E-1 ± 2.6E-2		1.3E-1 ± 8.6E-3	
	Anchor	3.3E+0 ± 5.7E-1		1.9E-1 ± 2.8E-2		9.0E-2 ± 2.6E-3	
Average periodic peak tension [N]	**WEC**	4.7E-1 ± 2.7E-2		1.5E-1 ± 4.5E-3		1.1E-1 ± 8.2E-4	
	Anchor	3.9E-1 ± 2.3E-2		9.7E-2 ± 8.8E-3		7.5E-2 ± 1.9E-3	
Maximum tension relative to neutral tension [N]	**WEC**	3.4E+0 ± 6.2E-1		2.2E-1 ± 2.7E-2		2.2E-2 ± 8.5E-3	
	Anchor	3.2E+0 ± 6.0E-1		7.3E-2 ± 5.0E-2		1.3E-2 ± 2.6E-3	
Rise time from neutral tension to initial maximum [s]	**Anchor**	1.945 ± 0.069					

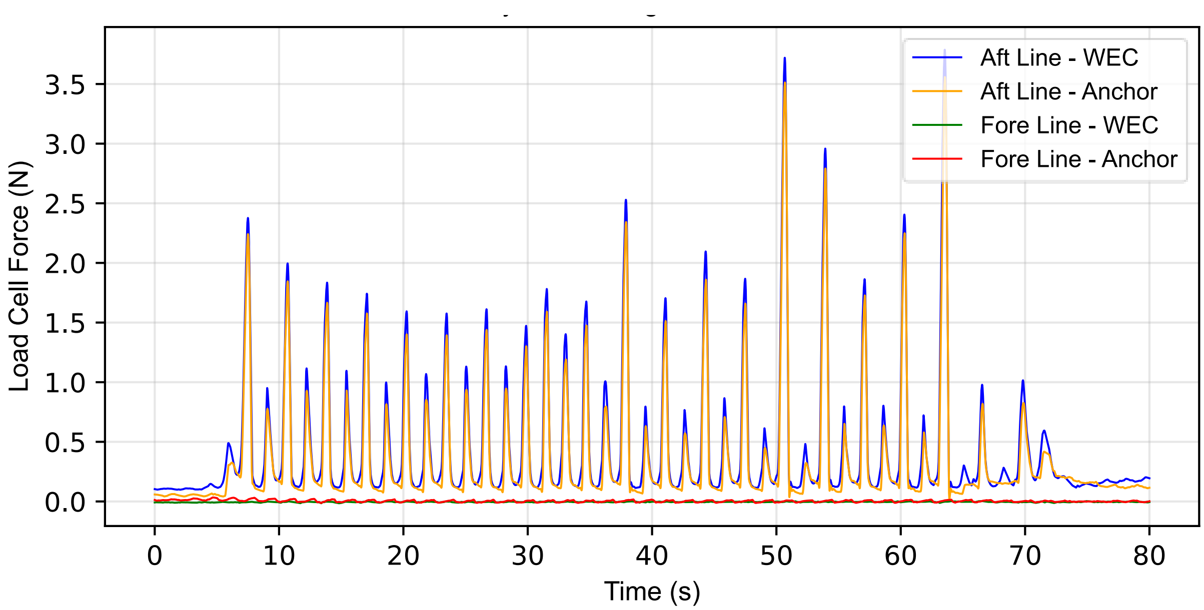

Figure 32. Plot of mooring loads for the semitaut polyester configuration with WEC load cells attached subjected to the 114.4 mm - 1.23 s wave case

7.4 Load Cell Configuration Comparison

For each mooring configuration and each wave case, it was found that the mooring loads were consistently lower for the cases with the WEC-side load cell connected. This is likely because the WEC load cell cable acted as an additional mooring point that takes some load from the intended mooring lines. A comparison of these values is shown in Figure 33. The case without load cells for the semitaut polyester configuration is not included.

It should also be noted that the neutral tension on each line did not align with the designed neutral tension. Furthermore, the neutral tensions are not in equilibrium. Because the WEC body is stationary during the beginning of the test, all forces acting on the body must add to zero; therefore, the tensions on the symmetric lines should be equal. This is shown in Figure 30 where neutral tensions on the two aft lines are significantly higher than those of the two fore lines. The difference is likely caused by the load cell cables pulling the device in the fore direction, which causes the aft lines to exert reaction forces to keep the device in equilibrium. Note that the anchor tension is expected to be lower than the WEC tension because of the mooring line's interaction with the seabed and the float.

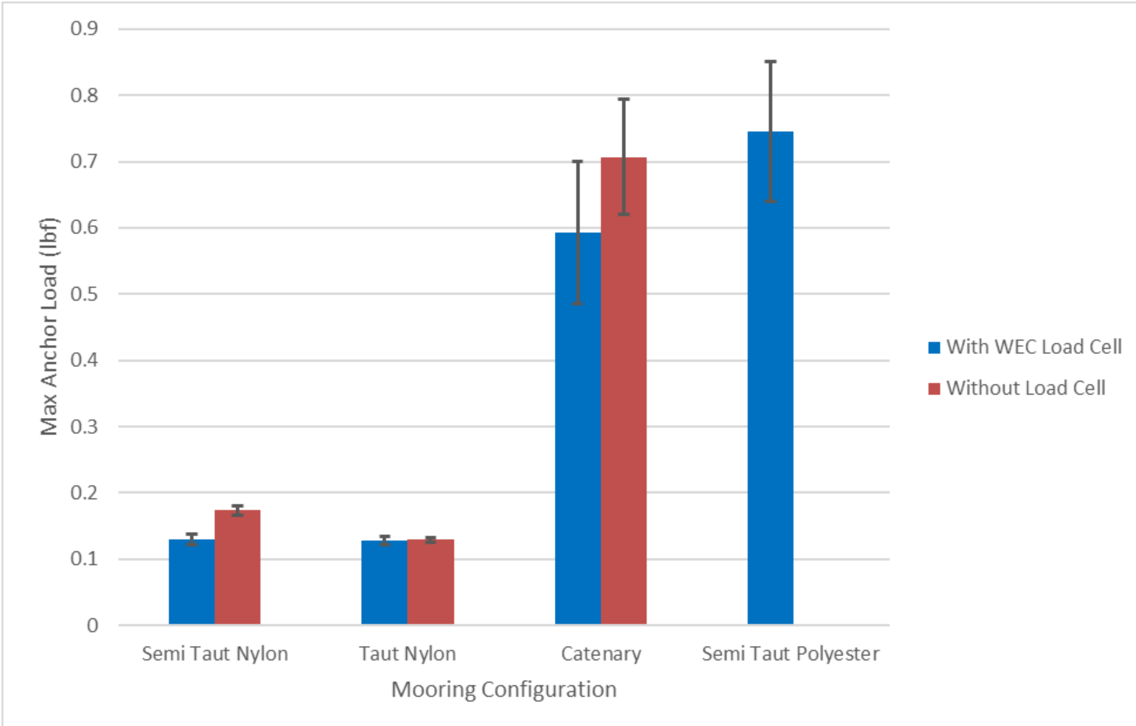

Figure 33. Maximum mooring line tension comparison between load cell configurations

8 Modeling

8.1 Background

The modeling effort aims to quantify the agreement between numerical models and tank testing data. Modeling was also used to better understand tank testing results of different small-scale WEC mooring systems. In this study, we conducted numerical simulations using mid-fidelity numerical models. We used the well-known open-source WEC modeling code WEC-Sim coupled to MoorDyn.

8.2 Numerical Modeling Setup

WEC-Sim version 7.0 was used to study different mooring line configurations. All simulations were simulated for the full-scale RM3 model, and outputs were scaled down for comparison purposes. Figure 34 displays the mesh used to compute the hydrodynamic coefficients of the current full-scale RM3 model using the solver WAMIT. There is a small physical gap between the float and spar geometries, which allows these two parts to move relative to one another. To avoid numerically high peak frequency from the water in this gap, a mesh was used to fill out the gap at the water surface. The hydrodynamic coefficient outputs are graphically plotted in Figure 35; the results are reasonable. Mean drift force coefficients were also computed in the WAMIT simulation using the surface control approach.

In the WEC-Sim model, a user wave elevation condition from three different recorded waves during tank testing was applied. As a new feature added to the WEC-Sim code for this study, a mean drift load, which is only available for regular and irregular wave boundary conditions, was adapted for the user wave elevation input. In this study, a dominant frequency from the user wave elevation input was derived to find a mean wave drift load with respect to this frequency. Instead of using a constant dominant wave amplitude derived from the user wave elevation, the instantaneous wave amplitude was used to precompute the mean drift load exerted on the WEC body. Additionally, viscous drag coefficients for the float and heave damping plate of 1.4 and 4.3, respectively, were applied from a previous study (Ruehl et al. 2014).

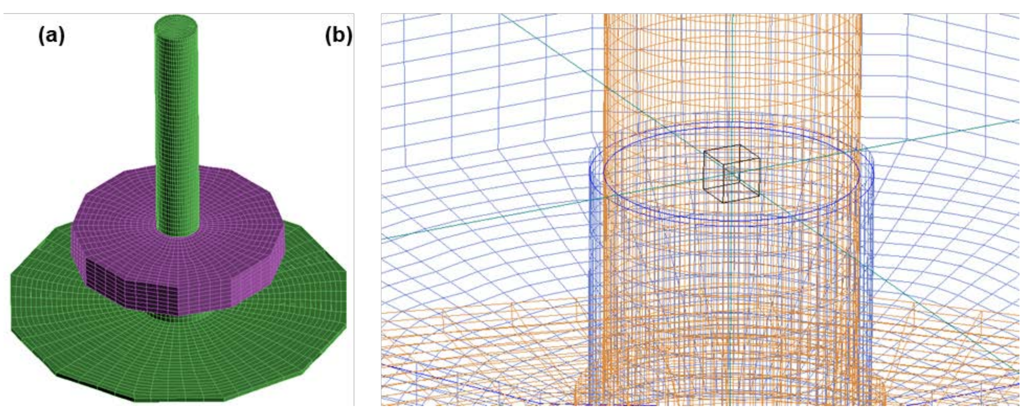

Figure 34. (a) Hydrodynamic mesh for WAMIT simulation and (b) a gap zoom-in area between spar and float bodies

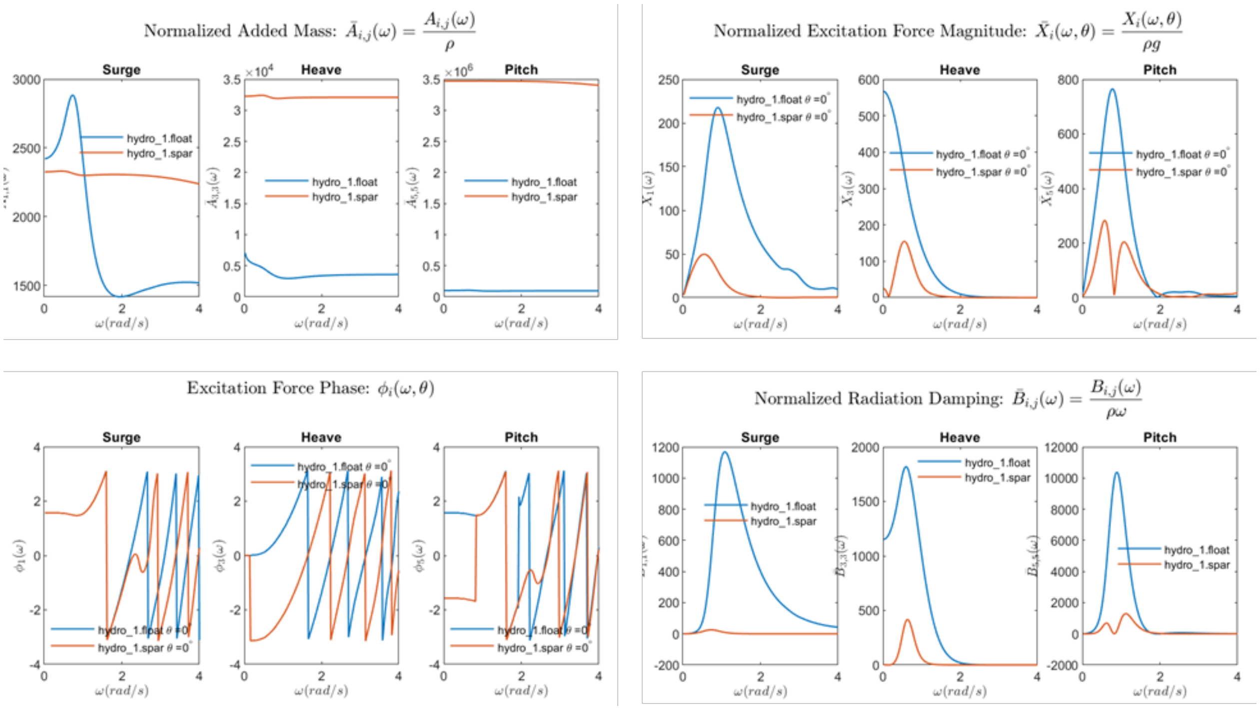

Figure 35. Hydrodynamic coefficients of the full-scale RM3 WEC device simulated by WAMIT (plotted by WEC-Sim BEMIO)

Figure 36 illustrates an example of the full-scale numerical RM3 WEC model with a catenary mooring line with a float buoy. Only a single mooring line is graphically displayed in this figure, but the WEC-Sim numerical setting included two symmetric lines (fore and aft mooring lines). The fairlead and anchor locations were the same for all other mooring configurations. The current numerical model setup, which was based on tank data, differs from the initial design (Figure 6) because of the actual model and its setting in the tank. Specifically, more draft lengths were considered in the current numerical model, which potentially leads to slightly higher hydrodynamic loads exerted on the WEC body.

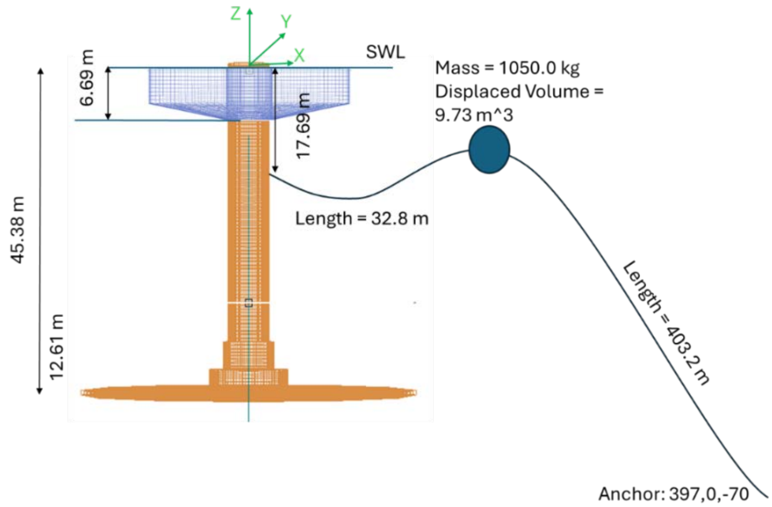

Figure 36. An illustration of the full-scale numerical RM3 WEC model with a catenary mooring line and a float buoy (same fairlead and anchor locations for all mooring configurations)

To ensure proper hydrodynamic coefficients used in this study, a validation study was conducted for a single-heave RM3 model and compared to previous data from both WEC-Sim and wave tank experiments (Ruehl et al. 2014). The dimensions of the current RM3 model are slightly bigger compared to those of the model in the previous study. Figure 37 shows a relative trend of heave response amplitude operator (RAO) output compared to that from the previous study. Slightly higher RAO output was expected due to a bigger geometry. These results enable us to confidently use the current hydrodynamic coefficients and numerical setting model for further validation steps.

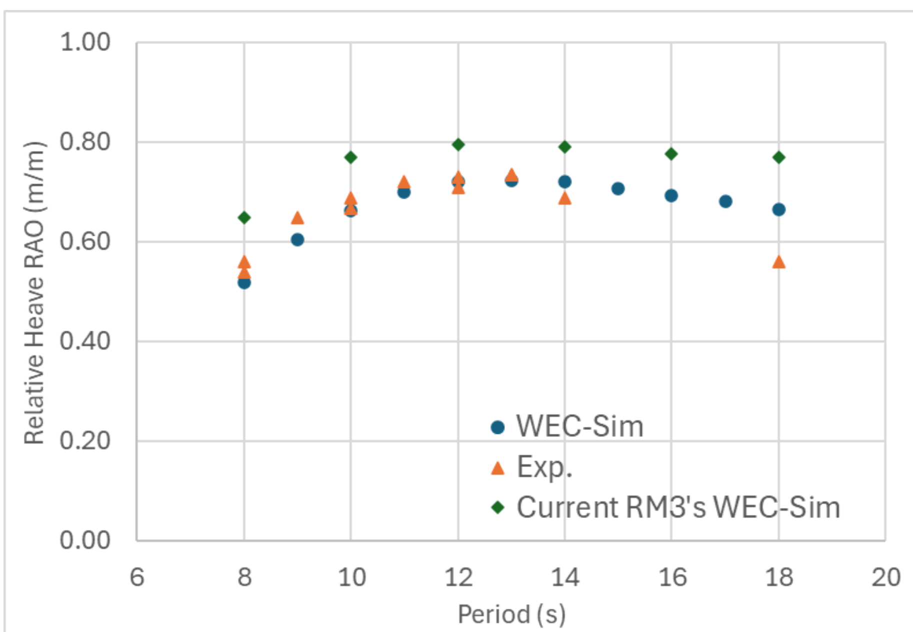

Figure 37. A comparison of hydrodynamic performance between the current tank-scale RM3 model versus previous data (both WEC-Sim and experimental data)

8.3 Comparison With Experimental Data

The experimental data using the 50-year extreme wave condition were used to tune the WEC-Sim input parameters, specifically viscous drag coefficients. Based on the viscous drag coefficients of 1.4 and 4.3, respectively, for the float and heave damping plate that were applied from the previous study, different drag coefficients in the horizontal direction were used in WEC-Sim (Figure 38). The first peak in fairlead tension for the catenary case varies within a range of 2.25–2.72 N. This first peak value seems to agree with the maximum tension for this test case presented in Table 23. Comparing continuing peaks of this upstream fairlead tension, it is interesting to see that the simulation with the float and spar drag coefficients of 4.2 and 0.5, respectively, shows a better agreement with the experimental data in both trend and peak values.

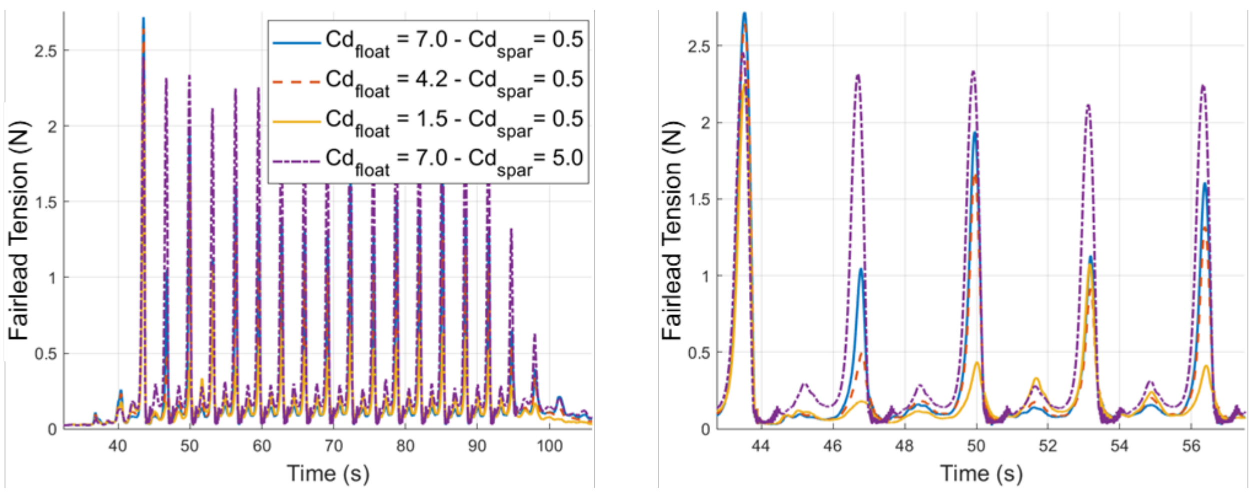

Figure 38. WEC-Sim simulation results for the WEC fairlead tension with different float and spar drag coefficients (catenary mooring case) wide view (left) narrow view (right)

The effect of mean wave drift load exerted on the WEC body was also investigated due to its low prediction at the beginning of this numerical effort. Figure 39 shows how simulation results are compared with and without the mean wave drift load, which is the second-order hydrodynamic pressure due to the first-order wave. As shown in the plot, the peak values are quite different between the two cases. The WEC-Sim simulation without the mean wave drift load effect predicted lower peaks as well as a higher rising time. Additionally, the subsequent peaks also have lower values compared to the WEC-Sim simulation with the mean wave drift load effect.

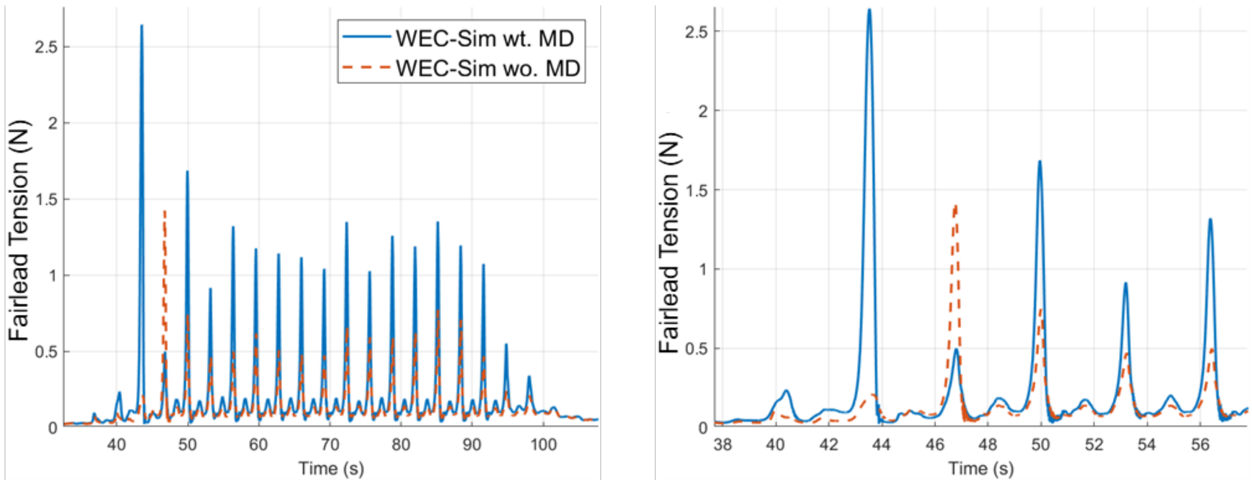

Figure 39. WEC-Sim simulation results of WEC's fairlead tension with different simulation settings including with and without mean drift load (MD)

Figure 40 compares WEC-Sim and experimental data for the upstream fairlead tension with the catenary mooring configuration for three different wave cases. As shown, the WEC-Sim simulation that includes the mean drift load effect predicts better agreement in both tension curve and maximum tension, specifically for the 50-year extreme wave case. For other wave cases, the tension curve predicted by WEC-Sim shows some agreement but has lower tension variation from the neutral tension (or initialization condition) to the first peak in the December mean wave case and higher tension variation from the neutral tension in the August mean wave case.

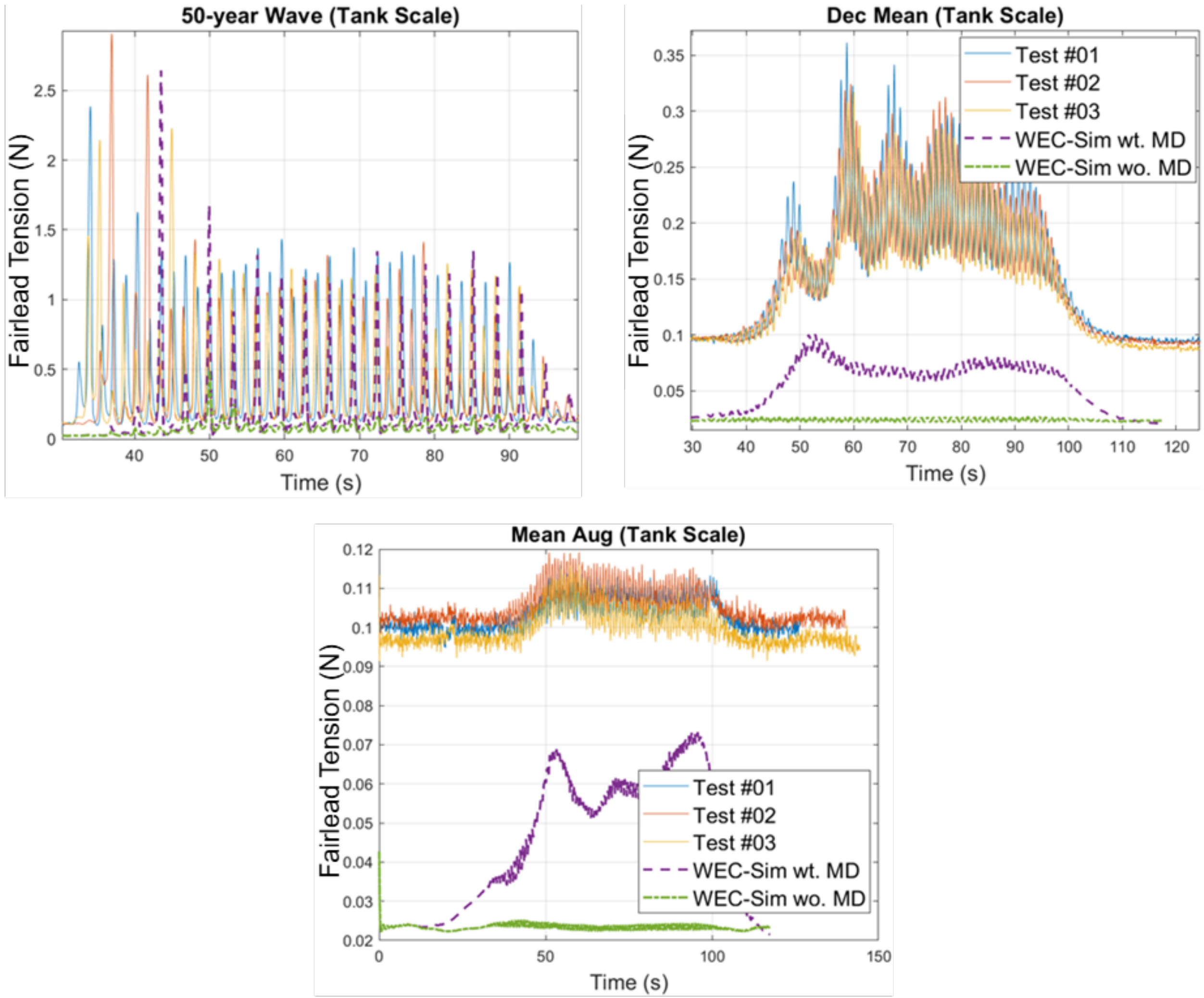

Figure 40. Comparison of WEC-Sim and experimental data for WEC fairlead tension with the catenary mooring configuration under different wave cases (50-year extreme, December mean, and August mean). Simulations are shown with and without the mean drift load effect (MD).

Similar WEC-Sim input parameters were used for other simulations with different mooring line configurations. Figure 41 compares WEC-Sim and experimental data for the upstream fairlead tension with the taut nylon mooring line configuration for three different wave cases. Similar to the catenary mooring configuration data, the WEC-Sim output including the mean drift load effect shows better agreement. The tension variation from the neutral tension (initialization condition) to the first peak shows better agreement between WEC-Sim and experimental data, specifically for the December and August mean wave cases.

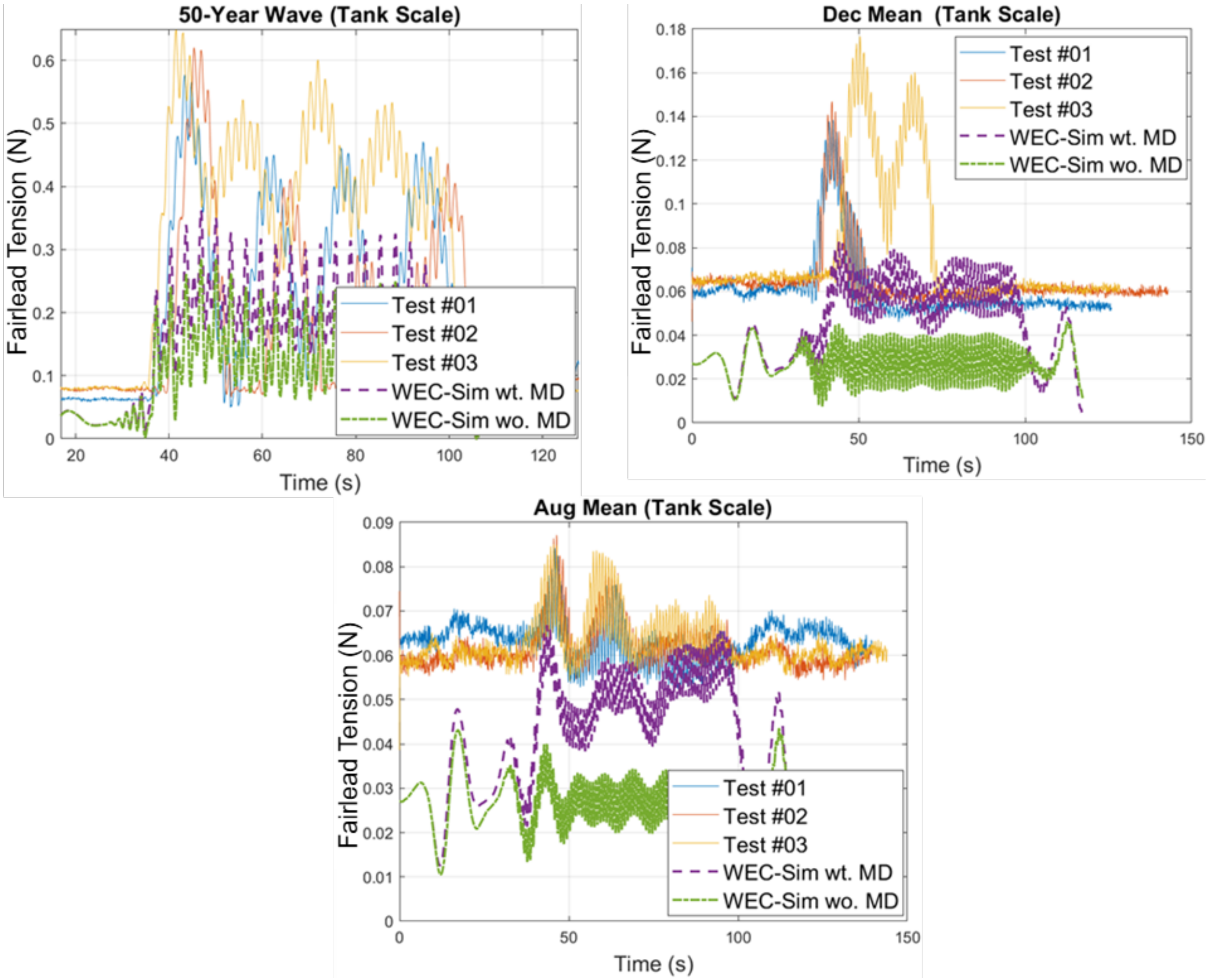

Figure 41. Comparison of WEC-Sim and experimental data for WEC fairlead tension with the taut nylon mooring configuration under different wave cases (50-year extreme, December mean, and August mean). Simulations are shown with and without the mean drift load effect (MD).

Lessons Learned

Numerical Wave Tank Testing Using WEC-Sim

Given the steps taken to improve validation results using WEC-Sim version 7.0, we learned the following:

- Overall, there is good agreement in both trend and maximum tension between WEC-Sim and experimental data under certain wave cases and mooring configurations. A calibration step was applied for a single wave case and mooring configuration, but it does not work for all cases. However, the peak value seems to vary less with a reasonable drag coefficient selection.
- A new feature added to WEC-Sim for a defined wave elevation was adapted to include a mean wave drift load. The results show significant improvement between WEC-Sim and experimental data, specifically in maximum tension and rising time. There are still

discrepancies between these two values for certain wave cases, which may have been caused by other factors, specifically from the tank testing. Alternatively, WEC-Sim could be improved to account for other terms of second-order wave loads (e.g., via quadratic full function or nonuniform drag coefficients from the waterline).

- During this project, we found that there is inconsistent mooring tension prediction between the Windows and Linux platforms, although we used the same input for a lower WEC-Sim version. Therefore, it is recommended to thoroughly check the code.

9 Conclusion

Throughout this work the complexity, difficulty, and practicality of recreating mooring systems at 1/100 scale has become apparent. Despite rigorous attention to detail in fabricating accurately scaled lines, the models were still not completely representative of the full-scale systems. This was due to numerous factors, including limited material selection making it difficult to find line and chain that was the correct diameter and weight, the need to add instrumentation and connectors in series with the lines, and springs not accurately recreating the nonlinear behavior of full-scale polymer mooring lines. The impact of the load cells on results was further enforced by the comparison of tests with and without the load cells attached to the WEC.

Despite the limitations in model building and testing, the maximum mooring line tension for each case was determined and compared to the estimated maximum load from WEC-Sim. The measured values were found to be repeatable with narrow standard deviations; however, the measured values were significantly different than the WEC-Sim estimates.

Lessons learned were noted throughout this work and are summarized in Appendix A. This report may be referenced for future work where scaled mooring systems will be built and tested. By considering the lessons learned in this study, it may be possible to attain better results that align with estimated and modeling results more closely. Overall, this study demonstrates that small-scale physical mooring models can provide valuable qualitative insight into relative mooring dynamic behavior and comparative performance across configurations. However, the numerous compounding model inaccuracies, instrumentation effects, and practical constraints make it difficult to obtain quantitatively accurate estimates of full-scale mooring loads.

Additional ongoing work aims to bypass these hurdles by replacing the scaled mooring systems with actively controlled hybrid mooring systems. Hybrid systems attempt to predict the mooring loads in real time using numerical models. The estimated loads are then applied to the device under test. While still being developed, these methods may prove superior to scaled model systems for some applications. However, hybrid systems rely on accurate numerical models, which may introduce additional error.

References

Dunkle, Gabrielle, Bryson Roberton, Gabriel García-Medina, and Zhaoqing Yang. 2020. *PacWave Wave Resource Assessment*. https://pacwaveenergy.org/wp-content/uploads/2021/11/PacWaveRA_updated.pdf.

Hall, Matthew, Stein Housner, Senu Sirnivas, and Samuel Wilson. 2021. *MoorPy: Quasi-Static Mooring Analysis in Python* [Computer software]. National Renewable Energy Laboratory. https://doi.org/10.11578/dc.20210726.1.

Housner, Stein, and Senu Sirnivas. 2023. *PacWave Anchoring and Mooring Study*. Golden, CO: National Renewable Energy Laboratory. NREL/TP-5000-84723. https://doi.org/10.2172/1996224.

Murdy, Paul, Charles Candon, Daniel Samborsky, David Miller, and Ryan Beach. 2024. *Polymer Additive Manufacturing for Marine Renewable Energy Applications: Best Practices, Research Trends, and Current Challenges*. Golden, CO: National Renewable Energy Laboratory. NREL/TP-5700-90930. https://doi.org/10.2172/2447830.

Neary, Vincent. S., Michael Lawson, Mirko Previsic, Andrea Copping, Kathleen C. Hallett, Alison LaBonte, Jeff Rieks, and Dianne Murray. 2014. "Methodology for Design and Economic Analysis of Marine Energy Conversion (MEC) Technologies." Presented at 2nd Marine Energy Technology Symposium, April 15–18, 2014, Seattle, WA. https://www.osti.gov/servlets/purl/1143279.

Ruehl, Kelley, Carlos Michelen, Samuel Kanner, Michael Lawson, and Yi-Hsiang Yu. 2014. "Preliminary Verification and Validation of WEC-Sim, an Open-Source Wave Energy Converter Design Tool." In *Proceedings of the ASME 2014 33rd International Conference on Ocean, Offshore and Arctic Engineering.* Volume 9B: Ocean Renewable Energy. V09BT09A040. https://doi.org/10.1115/OMAE2014-24312.

Appendix A. Summary of Lessons Learned

Model Building

3D printing is a good option for building wave tank models. When printing FDM parts, coating parts in epoxy works well for waterproofing. For smaller parts that do not require much strength, SLA printing is convenient. When designing models, considering the instrumentation wire route early in the design process is important. If possible, it is best to design the instrument cables with connectors so that the cables can be removed from the model easily.

Mass Properties

Mass properties varied between the CAD model and the physical model. It is best to take precise measurements of the physical model as built and use those to update a version of the CAD model "as built." This would require disassembling the model and weighing each component. Additionally, the center of mass, center of buoyancy, and moments of inertia should be measured using a custom-built apparatus.

While the platform system was largely successful, a few things could be improved. Figure 10 shows the gap between the two platforms. An alternate design that eliminated this gap would be preferable since some catenary configurations require contact with the seabed along the entire span of the mooring line. As seen in Figure 10, the catenary line is slightly overhanging this gap. Fortunately for this test, the device drifted in the fore direction (to the right) before the system was loaded, so the gap did not affect the results of the testing.

The vertical platform legs were made longer than necessary to allow the platform height to be adjusted for future tests. However, because these legs extend above the platform surface, they may contact the WEC. There would be more flexibility in the positioning of the WEC if these vertical legs did not extend above the platform surface.

Finally, the suction cup feet on the platforms were not ideal. They prevented the platforms from sliding on the tank floor; however, the suction cups flexed during large wave cases, causing the platforms to shift in the heave direction by 1–2 cm. While the effect of the shift was likely negligible on the experimental results, ideally, it would be eliminated. Using magnets or some other rigid attachment mechanism would be preferred.

Anchoring System

The suction cup anchoring system was not the ideal solution. They were difficult to place precisely on the platform from outside of the tank with the gripping jaw receiver. It was challenging to press down on the suction cup to get it to stick exactly in the intended location. Additionally, the load cell and instrument wire had to be managed. Since the load cells are exceptionally delicate, this procedure introduced a risk of damaging the load cells and causing them to vary from the OEM calibration. Rather than suction cups, a fixed mooring point would be better. However, this would require either entering the tank or removing the tables from the tank after each test. Additionally, the load cell instrument wire should be managed in a way that minimizes its influence on the load measurement. The wire running off the table may have added erroneous loads to the anchor tension measurements.

Mooring Line Construction

Accurately scaled mooring line materials are difficult to find. To produce a more accurately scaled model, custom line and chain should be sourced or fabricated. Connection points between the mooring lines and other components are difficult to recreate accurately at small scales. The terminations of the rope lines should be glued loops rather than tied knots. An iterative design approach should be taken to more accurately match the target elasticity of the lines. Some materials change length and properties when submerged, which must be considered when constructing the lines.

Instrumentation Cable Routing

Integrating load cells in line with the mooring lines proved to be especially difficult. For the anchor-side load cells, the wires could be fixed to the platform to reduce the effect of the weight of the cable on the load measurement. For the WEC-side load cells, it would be nearly impossible to run wires from the WEC to an external DAQ without influencing the test articles motion in some way. Integrating an onboard DAQ into the device could be one solution. In addition to these measures, the load cells should be tared while in place without any mooring line installed to compensate for the load cell wire weight and any other effects.

Load Cell Calibration

The load cells should be calibrated in the lab both before and after the tank testing. Because the only in-lab calibration was done after testing, it is uncertain whether the difference in calibration values was due to factors during testing or due to differences in the calibration procedure in the lab versus those used by the OEM. Additionally, the load cells should be calibrated before each day of testing to better inform how the sensor calibration changes throughout testing and alert the operator if a load cell was damaged.

Wave Tank Characterization and Wave Condition Selection

The actual wave height and period incident on the device were different than intended. This means that the intended scaled conditions from the PacWave site were not actually tested. In the future, more work should be done to produce wave profiles closer to the intended test cases, for example, through an iterative process of running waves, processing the results, and changing tank parameters. If the tank is unable to produce the correct wave profile, an alternatively scaled device may be tested so that the wave tank can produce the correct wave profile at the alternative scale.

Numerical Wave Tank Testing Using WEC-Sim

Given the steps taken to improve validation results using WEC-Sim version 7.0, the we learned the following:

- Overall, there is good agreement in both trend and maximum tension between WEC-Sim and experimental data under certain wave cases and mooring configurations. A calibration step was applied for a single wave case and mooring configuration, but it does not work for all cases. However, the peak value seems to vary less with a reasonable drag coefficient selection.
- A new feature added to WEC-Sim for a defined wave elevation was adapted to include a mean wave drift load. The results show significant improvement between WEC-Sim and experimental data, specifically in maximum tension and rising time. There are still discrepancies between these two values for certain wave cases, which may have been caused by other factors, specifically from the tank testing. Alternatively, WEC-Sim could be improved to account for other terms of second-order wave loads (e.g., via quadratic full function or nonuniform drag coefficients from the waterline).
- During this project, we found that there is inconsistent mooring tension prediction between the Window and Linux platforms, although we used the same input for a lower WEC-Sim version. Therefore, it is recommended to thoroughly check the code.

Appendix B. Instrumentation Specifications

Table B-1. Linear Potentiometer Specifications

Parameter	Specification
Sensor	Linear potentiometer
Qty	1
Manufacturer PN	MLP-75
Vendor	Mouser
Vender PN	824-MLP-75
Cost (2023)	$655.49
Input voltage	10 V
Signal type	Voltage divider
Stroke length	75 mm
Repeatability	0.01 mm

Table B-2. Load Cell Specifications

Parameter	Specification
Sensor	Submersible Miniature S-Beam Load Cell
Qty	4
Model	LSB210
Manufacturer PN	FSH04447
Vendor	Futek
Instrument Cost (2023)	$1,298.00
Calibration cost	$150.00
Input voltage	10 V
Rated output (RO)	2 mV/V
Capacity	10 lbf
Overload capacity	100 lbf
Linearity	0.2% RO
Weight	0.3 oz
IP rating	IP68
Water resistance	Up to 50 ft in fresh water for less than one week

Table B-3. Wave Height Sensor Specifications

Parameter	Specification
Sensor	Ultrasonic Wave Height Sensor
Qty	4
Model	ToughSonic 14 Level Sensor
Manufacturer PN	TSPC-N1S1-232
Vendor	Senix
Input voltage	10 V
Resolution	4,099 steps
Update rate	20 Hz

Table B-4. Motion Capture Camera Specifications

Parameter	Specification
Sensor	Qualisys Arqus A9 Cameras
Qty	4
3D resolution	0.002 in.
Frame rate	240 FPS

Table B-5. Analog Input Module (NI-9239) Specifications

Parameter	Specification
Sensor	Analog voltage input module
Model	NI-9239
Manufacturer	National Instruments
Analog input voltage range	-10 V to 10 V
Analog input resolution	24 bits
Maximum sample rate	50 kS/s/ch

Table B-6. Full-Bridge Analog Input (NI-9237) Specifications

Parameter	Specification
Sensor	Full-Bridge Analog Input
Model	NI-9237
Manufacturer	National Instruments
Analog input voltage range	-25 mV/V to 25 mV/V
Analog input resolution	24 bits
Maximum sample rate	50 kS/s/ch